Available online at www.sciencedirect.com
SCIENCE DIRECT®
Applied Catalysis B: Environmental 56 (2005) 9–35
APPLIED CATALYSIS B: ENVIRONMENTAL
www.elsevier.com/locate/apcatb

Review

Activity benchmarks and requirements for Pt, Pt-alloy, and non-Pt oxygen reduction catalysts for PEMFCs

Hubert A. Gasteiger*, Shyam S. Kocha, Bhaskar Sompalli, Frederick T. Wagner

General Motors Corporation, Fuel Cell Activities, Honeoye Falls, NY 14472, USA

Received 3 March 2004; received in revised form 15 May 2004; accepted 1 June 2004
Available online 5 November 2004

Abstract

The mass production of proton exchange membrane (PEM) fuel-cell-powered light-duty vehicles requires a reduction in the amount of Pt presently used in fuel cells. This paper quantifies the activities and voltage loss modes for state-of-the-art MEAs (membrane electrode assemblies), specifies performance goals needed for automotive application, and provides benchmark oxygen reduction activities for state-of-the-art platinum electrocatalysts using two different testing procedures to clearly establish the relative merit of candidate catalysts. A pathway to meet the automotive goals is charted, involving the further development of durable, high-activity Pt-alloy catalysts. The history, status in recent experiments, and prospects for Pt-alloy cathode catalysts are reviewed. The performance that would be needed for a cost-free non-Pt catalyst is defined quantitatively, and the behaviors of several published non-Pt catalyst systems (and logical extensions thereof), are compared to these requirements. Critical research topics are listed for the Pt-alloy catalysts, which appear to represent the most likely route to automotive fuel cells.

Keywords: Oxygen reduction catalysts; Non-platinum catalysts; Platinum–cobalt catalyst; Polymer electrolyte membrane fuel cell; Particle size effect; PEFC

Contents

* Corresponding author.
E-mail address: hubert.gasteiger@gm.com (H.A. Gasteiger).

0926-3373/$ – see front matter © 2004 Elsevier B.V. All rights reserved.
doi:10.1016/j.apcatb.2004.06.021

1. Introduction

Much progress has been made in reducing the platinum loading in H_2/air-fed polymer electrolyte membrane (PEM) fuel cells, resulting in currently applied membrane/electrode assembly (MEA) loadings of ca. 0.6–0.8 mg_{Pt}/cm^2_{MEA}, while at the same time power densities increased up to 0.7 W/cm^2_{MEA} at cell voltages as high as 0.68 V (i.e., at 58% energy conversion efficiency based on the thermodynamic H_2/air potential at 80 °C and near-ambient pressure) [1,2]. This corresponds to Pt-specific power densities of 0.85–1.1 g_{Pt}/kW, translating into 72–94 g of platinum for a ca. 85 kW fuel cell stack in a 75 kW_{net} automotive fuel cell system [3,4]. Even though this represents a significant reduction compared to PEMFC technology in the late 1990s, an approximately five-fold reduction of the amount of platinum contained in current PEMFC stacks is required for large-scale automotive applications, both for reasons of cost [5] and Pt supply limitations [6]. The latter two constraints would be met if the Pt-specific power density can be reduced to <0.2 g_{Pt}/kW at cell voltages of ≥ 0.65 V (an essential, yet often neglected requirement to maintain high fuel cell energy conversion efficiencies of >55%). Two strategies need to be pursued simultaneously to achieve this Pt-specific power density target: (i) increase of the MEA power density to 0.8–0.9 W/cm^2_{MEA} at ≥ 0.65 V by reducing mass-transport-induced voltage losses at high current densities and (ii) reduction of the Pt-loading in MEAs to ca. 0.15 mg_{Pt}/cm^2_{MEA} while maintaining high power densities.

In the first part of this paper, we will quantify the mass-transport-induced voltage losses, η_{tx}, obtained for state-of-the-art MEAs in order to define the voltage gains (i.e., the cell voltage at $\eta_{tx} = 0$) which, in principle, are achievable by proper engineering of electrodes, diffusion media, and flow-fields. While a reduction of η_{tx} to nearly zero at current densities of 1.5–2 A/cm^2 is not yet possible for stack components (MEAs, diffusion media, and flow-fields) currently used in the field, η_{tx} can be reduced significantly for novel materials/components tested on the research level as well as under certain operating conditions [7]. This analysis of the voltage gains projected for optimized fuel cell materials/components is one of the two critical elements in the technology development roadmap for achieving commercially viable platinum loadings for automotive PEM fuel cell applications.

Equally important is a stringent evaluation of the pathways for platinum-loading reduction in MEAs as well as of possible catalyst activity enhancements over state-of-the-art Pt/C catalysts. While lowering the Pt-loading for H_2-fed anode electrodes from today's 0.2–0.4 down to 0.05 mg_{Pt}/cm^2 is straightforward [8] due to the large activity of Pt toward the H_2-oxidation reaction [9], a lowering of today's cathode loadings of ca. 0.4 mg_{Pt}/cm^2 is limited by the poor activity of Pt for the oxygen reduction reaction (ORR) [10]. Therefore, decreasing the Pt-loading of cathode

electrodes is mainly pursued along two venues: (i) optimization of electrode structures so that the effect of reducing the cathode Pt-loading is limited to the purely kinetically predicted voltage loss over the entire current density range (i.e., ca. 20 mV for lowering the loading from 0.4 to 0.2 mg_{Pt}/cm^2) and (ii) implementation of more active Pt-alloy catalysts with reported mass activity gains (expressed in terms of A/mg_{Pt}) of $\geq$2 in both liquid electrolytes [11–13] and in PEMFCs [14,15].

By careful analysis of the above technology development roadmap, we will show that the target of 0.2 g_{Pt}/kW at $\geq$0.65 V cell voltage is indeed viable and can be accomplished by reducing the currently observed η_{tx} by 50% together with implementing Pt-alloy catalysts with a 2–4-fold increased mass activity over state-of-the-art Pt/C catalysts. Nevertheless, significant catalyst research is still required to develop activity-optimized and corrosion-resistant Pt-alloys.

To effectively develop improved ORR catalysts for PEMFCs, well-defined activity benchmarks and measurement methodologies for state-of-the-art Pt/C catalysts are required in order to assure that the activity of newly proposed catalysts can be compared and assessed unambiguously. Unfortunately this is not always the case, and activities reported in the scientific literature even for pure platinum catalysts often vary by an order of magnitude in both rotating disk electrode experiments on polycrystalline Pt (e.g., a 70 mV difference in half-wave potentials for the O_2-reduction under nominally identical conditions for the data shown in Fig. 2 of Ref. [12] versus Fig. 4 in Ref. [16]) as well as in PEMFC testing of Pt/C catalysts (see Table 3). Consequently, much effort is put into the development of novel catalysts, even though their activity compares poorly to that of industrially used state-of-the-art platinum catalysts, thus hampering the effectiveness of catalyst research. Therefore, we will present two methodologies for determining the mass activity (i.e., in units of A/mg_{Pt}) and the fundamentally more meaningful specific activity (i.e., in units of $\mu A/cm^2_{Pt}$) of Pt/C catalysts via (i) the thin-film rotating-disk electrode (TF-RDE) method for high-surface-area catalysts in aqueous electrolyte [13] and (ii) the testing of MEAs in H_2/O_2-fed single cells. Both approaches are shown to yield similar activities, the values of which will be compared to the literature values.

As discussed above, O_2-reduction activities in PEMFCs are reported to be a factor of 2–4 times larger for Pt-alloys/C (e.g., PtCo, PtCr, etc.) compared to Pt/C; so far, however, this technology has not been transferred into industrial applications. Our initial experiments demonstrated that as-received Pt-alloys indeed exhibit improved Pt-specific activities at very low current densities (<0.1 A/cm^2) in H_2/O_2-fed MEAs, but enhancement at higher current density is frequently not observed. Some of these discrepancies may be due to the leaching of the alloys' base-metal components into the acidic ionomeric electrolyte, as was suggested by Mukerjee and Srinivasan [15] and will be discussed in Section 4. Owing to the generally lower metal dispersion of Pt-alloys/C compared to Pt/C, their more application-relevant mass activity enhancement is unfortunately less than their specific activity gain, putting a strong emphasis on the development of high-dispersion Pt-alloy catalysts.

While our analysis of the technology development roadmap toward a <0.2 g_{Pt}/kW target (at $\geq$0.65 V) shows that this can be accomplished by means of incremental improvements of fuel cell components and the implementation of known, but improved Pt-alloy cathode catalysts, the scientific search for Pt-free cathode catalysts is intriguing as they would potentially reduce MEA cost to even lower levels. While the overall research efforts in this area were rather modest over the past decade, a few interesting concepts have been pursued [17–21]. Even though their ORR turnover frequency (TOF) is lower than Pt, the argument could be made that orders of magnitude of lower TOFs (turnover frequencies, i.e., electrons/site/s) might be acceptable from a cost point of view for an essentially ''costless'' catalyst. We will present an analysis to quantify this statement in the context of the constraints placed upon automotive PEMFCs: (i) high power densities (i.e., ca. 0.8–0.9 W/cm^2_{MEA}) are essential not only to meet the tight packaging requirements for automotive applications, but also to reduce the per-kW cost of other PEMFC stack components (e.g., membranes, diffusion media, bipolar plates) and (ii) cell voltages of ca. $\geq$0.65 V at full power are required not only for high energy conversion efficiency (one of the major advantages of PEMFCs over internal combustion engines), but equally important for minimizing the difficulties associated with heat-rejection from a PEMFC vehicle [3]. Since high power densities require thin electrodes (on the order of less than 100 μm) to avoid excessive mass-transport-related voltage losses, η_{tx}, the critical *figure-of-merit* for ''costless'' cathode catalysts is the product of TOF and site density at $\geq$0.65 V, rather than merely the TOF often used in the case of currently applied high-site-density Pt/C catalysts (usually 40–60 wt.% of Pt on carbon support). This ''costless'' catalyst *figure-of-merit* may alternatively be expressed in units of $A/cm^3_{electrode}$, resulting in a development target of ca. 100 $A/cm^3_{electrode}$ at 0.90 V, 80 °C, and 100 kPa_{abs} O_2. A comparison with the literature will demonstrate how closely this target can be met with current Pt-free catalysts.

In summary, we will attempt to (i) outline the technology development roadmap for obtaining Pt-specific power densities of <0.2 g_{Pt}/kW, (ii) quantify the activity benchmarks of *state-of-the-art* platinum cathode catalysts by using two different experimental methods, (iii) describe the current status of Pt-alloy cathode catalysts and their development needs in terms of activity and stability, and (iv) provide activity benchmarks for the ''costless'' cathode catalysts under the constraints placed on automotive PEM fuel cell applications.

2. Experimental

2.1. MEA preparation

2.1.1. General MEA and diffusion media preparation

An MEA consists of anode and cathode electrodes, anode and cathode diffusion media (also referred to as substrates), and a proton-conducting membrane. Principally two different methods are used to prepare an MEA consisting of these five layers (for details, see Ref. [1]): (i) direct application of electrodes onto the membrane, resulting in a so-called catalyst-coated membrane (CCM), which is then sandwiched between two diffusion media or (ii) direct application of electrodes onto pre-treated diffusion media (i.e., substrates), resulting in so-called catalyst-coated substrates (CCS), which then are laminated onto each side of a membrane.

Catalyst-coated membranes for both small-scale (50 cm^2) and short-stack testing (465 cm^2) were prepared by an identical procedure [10,22] with the exception of the CCMs described in Section 2.1.2 which were prepared from commercially available materials in order to allow benchmarking at different laboratories. Different ionomers, membranes, and catalysts were used and are specified in the respective figure legends. Ionomer/carbon weight ratios were ca. 0.8/1, unless specified otherwise. Carbon-supported Pt catalysts and ionomer solutions (ca. 900 EW (equivalent weight in $g_{polymer}/mol_{H+}$) perfluorosulfonic acid (PFSA) ionomers) were used to fabricate thin-layer electrodes which were transferred via a decal method onto 25–50 μm thick PFSA membranes with various EWs. All catalyst loadings are referenced to the geometric surface area of the membrane, labeled as mg_{Pt}/cm^2 (note: cm^2 always refers to the geometric electrode area). Specific catalyst loadings are given in the figures and figure captions, labeled as anode/cathode loadings.

Gas-diffusion media (DM) were treated in-house and are based on carbon fiber paper substrates (Toray, Inc., Japan). Both anode and cathode DMs were teflonated and additionally processed using a proprietary surface treatment. Single cells (50 cm^2 active area) and a ca. 20-cell short stack (465 cm^2 active area) were assembled by sandwiching CCMs between the appropriate DMs and applying an average compression of approximately 1500 kPa_{abs} onto the active area.

2.1.2. CCMs and diffusion media prepared with commercial components

Various carbon-supported catalysts, ionomer solution (SE20092: 20 wt.% Nafion solution (1000 EW), Dupont) and *iso*-propanol (Aldrich, HPLC grade) were used to prepare catalyst inks. The mass ratio of solids (ionomer and catalyst) to liquids (ionomer solution solvents and *iso*-propanol) in the catalyst inks was ca. 0.13/1, while targeting an ionomer/carbon mass ratio of 1/1. Inks were ball-milled in Nalgene® bottles for 12–20 h using zirconia beads (US Stoneware, Inc., East Palestine, OH). Subsequently, they were slot-coated onto 50 μm thick PTFE decals (Enflo Corp., NJ, USA) using 50 cm^2 area slots cut into Kapton-HN® films of thicknesses appropriate to obtain the desired catalyst loadings (ca. 75 μm). A lab vacuum table was used to hold the decal flat with a mild vacuum while the Kapton-HN® film with the slot was placed on top of the decal. Each decal was coated two times with intermediate drying at ca. 80 °C under an infrared lamp. Catalyst loadings were calculated by weighing the decals before (blank) and after coating the catalysts.

The decal transfer process consisted of hot-pressing the 50 cm^2 catalyst-coated PTFE sheets onto the polymer electrolyte membrane (solution-cast 50 μm 1100 EW Nafion112®) at 146 °C and 1700 kPa_{abs} for 6 min. Uniformity in pressure distribution during decal transfer was obtained by using Gylon® pressure relief films (Garlock Corp.). The CCMs were sandwiched between commercially available gas-diffusion media (type 20BC, SGL Corp.) and assembled into a 50-cm^2 cell (graphite flow-fields from Poco Graphite Company). The cell compression was set such that ca. 20% compression of the diffusion media was obtained. More details on CCM preparation and cell build can be found elsewhere [23].

2.2. Catalyst surface areas and catalyst utilization in CCMs

The intrinsic Pt catalyst surface area (sometimes referred to as the electrochemical area (ECA) [24]), $A_{Pt,cat}$, was determined by supporting a thin film of catalyst on a glassy-carbon disk electrode and integrating the hydrogen adsorption/desorption areas of the cyclic voltammogram (assuming 210 $\mu C/cm^2_{Pt}$ after double-layer correction) obtained at 20 mV/s in either 0.1 M $HClO_4$ or 0.5 M H_2SO_4 at room temperature. Care was taken to limit the positive potential window to 1.2 V versus RHE (reversible hydrogen electrode potential in the same solution). Catalyst dispersions were prepared by ultrasonically dispersing 20–50 mg catalyst in 50 ml of an aqueous solution containing 10–20 ml of *iso*-propanol and 0.2 ml of a 5 wt.% Nafion® solution. Twenty microliters of these inks was dispersed onto 5 or 6 mm glassy-carbon disk electrodes and dried either at room temperature or in a warm air stream. Intrinsic catalyst surface areas, $A_{Pt,cat}$, are reported in terms of m^2/g_{Pt} [10] and are listed for four different Pt-catalysts in Table 2.

When fabricating electrodes with solid polymer electrolytes, it is not guaranteed that all of the Pt surface area of the catalyst (i.e., $A_{Pt,cat}$) is available for the electrochemical reaction due to either insufficient contact with the solid electrolyte or due to electrical isolation of catalyst particles from each other by a film of the electrically non-conducting solid electrolyte. Therefore, the Pt-surface area measured by cyclic voltammetry in an MEA, $A_{Pt,MEA}$, using the so-called *driven-cell* mode [10] may be substantially smaller than the intrinsic surface area of a catalyst, $A_{Pt,cat}$, and the ratio of

$A_{Pt,cat}/A_{Pt,MEA}$ is often referred to as MEA catalyst utilization, u_{Pt}. Reported values range from 60–70 [24] to 75–98% (see Table 2, and other references [1,10]), depending on the MEA preparation.

2.3. H_2-crossover corrections

Due to the low but finite solubility and diffusivity of H_2 in the ionomer [1], H_2 permeates from the anode compartment of a PEMFC to the cathode, where it is oxidized electrochemically at the typical cathode potential (0.5–1.0 V versus RHE, depending on the current density). The resulting parasitic H_2 oxidation current density is generally referred to as H_2-*crossover current density*, i_x, and can be determined experimentally using the above-described driven-cell mode, by polarizing the N_2-purged cathode compartment at >+0.4 V with respect to the H_2-purged anode compartment (at >0.4 V, the resulting H_2 oxidation current density is purely limited by the H_2 permeation rate). This method is described in detail in Ref. [1] where it is also shown that the observed H_2-crossover current density increases with increasing H_2 partial pressure and increasing cell temperature. For this study, H_2-crossover current densities were measured under the operating conditions (i.e., temperature and H_2-partial pressure) and catalyst activities were evaluated on the basis of H_2-crossover corrected current densities, i_{eff} (i.e., $i_{eff} = i + i_x$, with i_x being on the order of 2–5 mA/cm^2).

For the evaluation of kinetic activities it is also crucial that the CCMs assembled in the fuel cell hardware do not exhibit ohmic shorts, which are generally expressed in terms of Ω cm^2 and can be measured in situ [1]. Shorting resistances in this study were always $\gg$1000 Ω cm^2, so that current density measurement errors are $\ll$1 mA/cm^2 and can be neglected.

2.4. Fuel cell testing

Fuel cell stations from Fuel Cell Technology (Los Alamos, NM) or Hydrogenics (Mississauga, Canada) were used to test 50 cm^2 active-area MEAs. Pure oxygen and air were used as cathode reactants and pure H_2 as anode reactant (all gases of 99.99% purity). Stoichiometric flow rates of anode (s = 2) and cathode (s = 9.5 for O_2 and s = 2 for air) reactants were used at current densities $\geq$0.2 A/cm^2 and constant flows (corresponding to 0.2 A/cm^2 flows) were used at <0.2 A/cm^2. Reactant humidification was achieved by water-bubblers, the temperatures of which were calibrated to yield the quoted relative humidity (RH) values. Cell resistances as a function of current density (i.e., the sum of the proton-conduction resistance in the membrane and the various electronic resistances (bulk and contact resistances)) were determined using an AC perturbation of 1 kHz. For each data point, the cell voltage was stabilized over 15 min and data were averaged over the last 5 min. Multiple-path serpentine flow-fields (two and three parallel channels for the anode and cathode, respectively) machined into sealed graphite blocks (Poco) were used for 50 cm^2 testing. The flow-field channel width was approximately 0.8 mm with a channel/land width ratio of 1.3/1.

For stack testing, 465 cm^2 active-area MEAs with different catalyst loadings were tested in the same stack. Performance data shown in this work usually represent the average of four nominally identical samples in the same short stack (ca. 20 cells) and the quoted stoichiometric flows apply to all current densities. Cell resistances in the short stack were measured the same way as in the above-described 50 cm^2 testing. The flow-field configuration of the short stack is proprietary; for short-stack testing Hydrogenics teststands were used.

2.5. Rotating disk measurements

Rotating disk electrode (RDE) measurements were conducted on both a polycrystalline Pt-disk (0.196 cm^2) as well as on high-surface-area catalysts deposited on glassy-carbon disk electrodes (0.283 cm^2 area), mounted in an interchangeable RDE holder (Pine Instruments, USA). A Pt-foil counter-electrode and a saturated calomel reference electrode (separated by an electrolyte bridge) were used in a standard three-compartment electrochemical cell. All potentials, however, are reported in terms of the reversible hydrogen electrode (RHE) scale, calibrated before each measurement at each temperature via H_2 oxidation/reduction measurements on platinum [13,23]. For the thin-film RDE (TF-RDE) measurements, carbon-supported catalysts and Pt-black were put onto polished glassy-carbon disks by applying 20 μl of a well-dispersed catalyst ink, prepared as described in Section 2.2. After drying at room temperature, catalyst loadings ranged from ca. 12 μg_{Pt}/cm^2 for carbon-supported catalysts to ca. 50 μg_{Pt}/cm^2 for Pt-black.

Pt-surface areas were determined by cyclic voltammetry (see Section 2.2) in either 0.5 M H_2SO_4 or 0.1 M $HClO_4$ at room temperature and 20 mV/s. Oxygen reduction activities were measured at 1600 rpm and 60 °C in 0.1 M $HClO_4$ (GSF Chemicals, Inc., Ohio, USA, double distilled 70 wt.% $HClO_4$ with <0.1 ppm chloride) for positive-going potential sweeps between 0 and 1.0 V versus RHE at low sweep rates (5 and 20 mV/s) in order to minimize the interference from capacitive currents. Measured currents were mass-transport-corrected in order to determine mass and specific activities. Details on the TF-RDE method are described elsewhere [13,23,25].

3. Results

3.1. Projections of Pt-specific power densities

3.1.1. Determination of voltage loss terms in state-of-the-art MEAs

Fig. 1 shows the MEA performance in a 50-cm^2 single cell using state-of-the-art non-commercial components

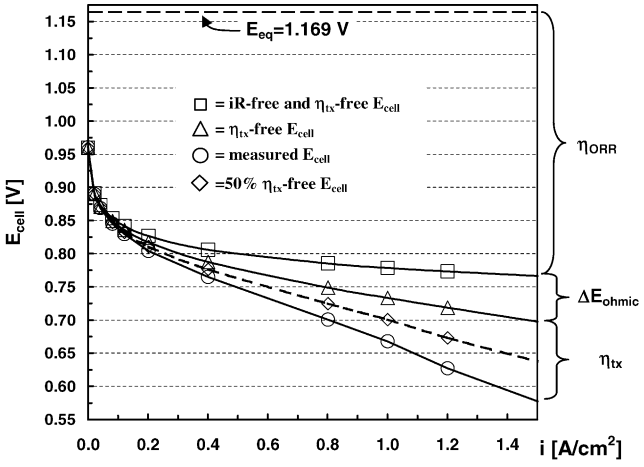

Fig. 1. (a) Circular symbols: 50 cm^2 single-cell H_2/air performance at T_{cell} = 80 °C (80 °C dew points, i.e., 100% RH) at a total pressure of 150 kPa_{abs} and stoichiometric flows of s = 2.0/2.0 (controlled stoichiometric flows for $i \geq 0.2$ A/cm^2; 0.2 A/cm^2 flows at $i < 0.2$ A/cm^2). Catalyst-coated membrane (CCM) based on a ca. 25-μm low-EW membrane (ca. 900 EW) coated with electrodes consisting of ca. 50 wt.% Pt/carbon (0.4/0.4 mg_{Pt}/cm^2 (anode/cathode)) and a low-EW ionomer (ca. 900 EW; ionomer/carbon ratio = 0.8/1). (b) Square symbols: E_{cell} vs. i for the mass-transport-free and ohmically corrected (i.e., iR-free) E_{cell}/i-curve shown in (a). In situ measurements of the high-frequency resistance vs. current density were obtained at 1 kHz (ranging from 45 to 55 mΩ cm^2) and used for the ohmic correction. (c) Triangular symbols: Addition of the ohmic losses, ΔE_{ohmic}, to the polarization curve shown in (b). (d) Diamond symbols: E_{cell}/i-curve shown in (a) corrected for 50% of the mass-transport losses.

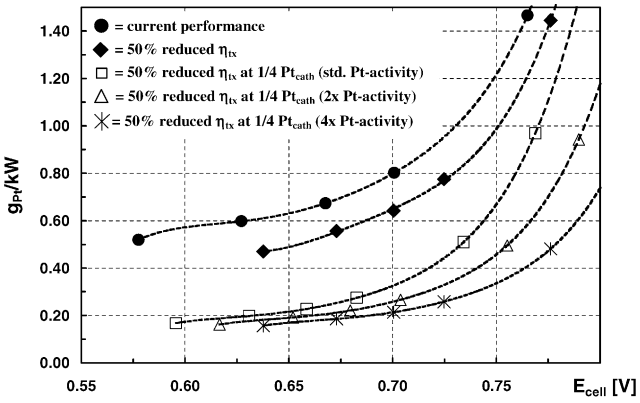

Fig. 2. Pt-specific power density [g_{Pt}/kW] vs. cell voltage, E_{cell}, based on the performance curves shown in Fig. 1a ("current performance") and Fig. 1d ("50% reduced η_{tx}"). It is assumed that the cell performance can be maintained at a reduced anode loading of 0.05 mg_{Pt}/cm^2 (see text). (a) Circular symbols: g_{Pt}/kW vs. E_{cell} for the uncorrected cell performance curve in Fig. 1a. (b) Diamond symbols: g_{Pt}/kW vs. E_{cell} assuming a 50% reduced η_{tx} as shown in Fig. 1d. (c) Square symbols: g_{Pt}/kW vs. E_{cell} assuming a 50% reduced η_{tx} and a four-fold lower Pt-loading (0.05/0.1 mg_{Pt}/cm^2), without catalyst improvement (i.e., E_{cell}-loss of 42 mV at all i's). (d) Triangular symbols: g_{Pt}/kW vs. E_{cell} assuming a 50% reduced η_{tx} and a four-fold lower Pt-loading (0.05/0.1 mg_{Pt}/cm^2), with two-fold catalyst activity improvement (i.e., E_{cell}-loss of 21 mV at all i's). (e) Star symbols: g_{Pt}/kW vs. E_{cell} assuming a 50% reduced η_{tx} and a four-fold lower Pt-loading (0.05/0.1 mg_{Pt}/cm^2), with four-fold catalyst activity improvement (i.e., no E_{cell}-loss).

(ca. 25 μm thick membranes (ca. 900 EW), ca. 900 EW ionomer in the electrodes, and advanced carbon-fiber-based diffusion media with proprietary surface treatment) at a 0.4/0.4 mg_{Pt}/cm^2 Pt-loading (using a 47% Pt/C catalyst (TKK) on a proprietary carbon support, with a Pt surface area of ca. 75 m^2/g_{Pt} and an MEA Pt utilization of ca. 80% (see 2nd column of Table 2)). At 80 °C and 150 kPa_{abs} using fully humidified H_2/air reactants (s = 2/2), the power density at 0.65 V amounts to 0.71 W/cm^2, translating into a Pt-specific power density of 1.1 g_{Pt}/kW. While this is clearly far above the target value of <0.2 g_{Pt}/kW, we showed previously that the identical performance can be obtained at a reduced anode loading of 0.05 mg_{Pt}/cm^2 [8] owing to the high catalytic activity of Pt toward the H_2 oxidation reaction of pure H_2-fuel (this, unfortunately, is not true in the case of CO-contaminated H_2-reformate). Therefore, considering that the same performance is obtained at the reduced Pt-loading of 0.05/0.4 mg_{Pt}/cm^2, the Pt-specific power density under the same operating conditions reduces to a value of 0.63 g_{Pt}/kW at 0.65 V. Fig. 2 shows the dependence of the Pt-specific power density as a function of cell voltage (solid circles), demonstrating that even at lower cell voltages only marginal reductions of the Pt-specific power density can be obtained (ca. 0.5 g_{Pt}/kW at 0.60 V), so that other measures are required for achieving the automotive target of <0.2 g_{Pt}/kW.

In order to decide how to approach a further reduction of the Pt-specific power density, it is essential to understand the various voltage loss terms, i.e., to quantify the voltage loss contributions from: (i) the sluggish O_2 reduction kinetics, the so-called cathode overpotential, η_{ORR}, (ii) the ohmic losses, ΔE_{ohmic}, due to both electronic contact resistances between the flow-fields and the diffusion media as well as the ohmic resistance due to proton conduction through the membrane, and (iii) the mass-transport losses, η_{tx}, incurred by poor O_2-transport through the diffusion medium and the electrode layer. Based on a more detailed analysis, we showed previously that both kinetic and mass-transport losses of the hydrogen electrode can be neglected. Therefore, the cell voltage, E_{cell}, of a H_2/air fuel cell can be described as [5,8,10]:

$$E_{cell} = E_{rev(p_{H_2}, p_{O_2}, T)} - \Delta E_{ohmic} - \eta_{ORR} - \eta_{tx} \quad (1)$$

The first term on the right-hand side of Eq. (1) is the reversible H_2/O_2 cell voltage, which depends on the partial pressures of the reactants and the cell temperature, equating to 1.169 V under the operating conditions of Fig. 1 [26]. The ohmic voltage loss, ΔE_{ohmic}, can be measured directly via either current-interrupt or high-frequency resistance measurements. For the data shown in Fig. 1, the in situ measured ohmic resistance, R_Ω, varied from 45 to 55 mΩ cm^2, consistent with a value calculated from independent ex situ measurements of both the contact resistance between flow-field plates and the diffusion media as well as the membrane conductivity, each contributing approximately 50% to the

measured overall resistance [10]. Therefore, the ohmically corrected cell voltage, $E_{iR\text{-free}}$, can be determined directly from the experimental data:

$$E_{iR\text{-free}} = E_{\text{cell}} + \Delta E_{\text{ohmic}} = E_{\text{cell}} + iR_{\Omega}$$
$$= E_{\text{rev}(p_{H_2}, p_{O_2}, T)} - \eta_{\text{ORR}} - \eta_{\text{tx}} \quad (2)$$

At 1.5 A/cm^2, the ohmic-resistance-induced voltage loss, ΔE_{ohmic}, amounts to only 70–80 mV. Membranes with improved conductivity and improved contact resistance between flow-fields and diffusion media could lead to slightly reduced ohmic losses in future designs, but losses of less than 50 mV at 1.5 A/cm^2 (i.e., <35 mΩ cm^2) are unlikely to be achieved. Nevertheless, the ca. 590 mV deviation between the measured cell voltage (ca. 580 mV) and the thermodynamically predicted reversible cell voltage (ca. 1170 mV) which is seen in Fig. 1 is largely due to the other two terms in Eq. (2), viz., η_{ORR} and η_{tx}, so that understanding the nature of these losses as well as reducing these losses is most critical for improving the cell performance.

We demonstrated in previous work [5,8,10] that the *iR*-free cell voltage of state-of-the-art MEAs operating on H_2/air at low current densities (≤0.1 A/cm^2) is controlled solely by the voltage loss due to the O_2 reduction kinetics, i.e., by the η_{ORR} term in Eq. (2). We furthermore showed that the cathode overpotential term for Pt-catalysts follows a *Tafel-equation*, relating the *iR*-free voltage loss to the logarithm of the H_2-crossover-corrected current density, i_{eff}:

$$\eta_{\text{ORR}} \propto b \log(i_{\text{eff}}) \quad (3)$$

where b is the so-called *Tafel-slope* with a value of 70 mV/decade at 80 °C and 65 mV/decade at 60 °C. Therefore, a conceptual polarization curve which would be obtained in the absence of mass transport and ohmic resistances (i.e., $\eta_{\text{tx}} = \Delta E_{\text{ohmic}} = 0$) can be constructed by extrapolating the *iR*-free cell voltage obtained at low current densities (<0.1 A/cm^2) by means of Eq. (3), resulting in a loss of 70 mV for every 10-fold increase in current density. This is shown by the square symbols in Fig. 1, demonstrating the well-known fact, that the cathode overpotential loss, η_{ORR}, is the major contributor to the deviation between the thermodynamically predicted reversible cell voltage and the actually obtained cell voltage [27], amounting to ca. 400 mV at 1.5 A/cm^2 (see Fig. 1).

Finally, adding the measured ohmic losses, ΔE_{ohmic}, to the purely kinetically controlled conceptual polarization curve (square symbols in Fig. 1), yields the mass-transport-free (i.e., η_{tx} =0) cell voltage (triangular symbols in Fig. 1). This polarization curve demonstrates that, even with the ohmic loss incurred by current membranes and bipolar plate materials, cell voltage gains of 120 mV at 1.5 A/cm^2 could be obtained for properly designed flow-fields, diffusion media, and electrode structures. As was mentioned in the Section 1, η_{tx} can be reduced significantly with novel, not yet commercially available materials/components as well as under certain operating conditions. Based on published data [2,7] as well as on unpublished data from General Motors' R&D, it is anticipated that the mass-transport losses shown in Fig. 1 will soon be reduced by at least 50% at current densities as high as 1.5 A/cm^2, facilitated mainly by improved handling of liquid water in flow-fields, diffusion media, and electrode structures (note that the calculated mass-transport losses due to O_2 gas-phase diffusion through the diffusion medium and the electrode in the absence of liquid water amounts to only ca. 10 mV at 1.5 A/cm^2). This anticipated cell voltage performance is shown as dashed line in Fig. 1 (diamond symbols), and will serve as basis to establish the near-term improvements in both MEA power density and Pt-specific power density with state-of-the-art Pt/C cathode catalysts. As shown in Fig. 2 (solid diamond symbols), a 50% reduction in mass-transport losses only slightly reduces the g_{Pt}/kW, resulting in a value of 0.48 g_{Pt}/kW at 0.65 V. However, reduction of η_{tx} does also increase the MEA power density to 0.91 W/cm^2 at 0.65 V (see Table 1, second row) which positively impacts packaging of the fuel cell stack in a vehicle and, more importantly, reduces the cost of other stack components (bipolar plates, diffusion media, membranes).

3.1.2. Impact of cathode Pt-loading reduction and increased catalyst activity

The above analysis clearly demonstrates that significant Pt-loading reductions on the cathode are required to meet the <0.2 g_{Pt}/kW target. One approach may be to reduce the Pt-loading and accept the concomitant loss in cell voltage. If the mass-transport losses do not increase as the Pt-loading is reduced, the change in cell voltage as a function of cathode Pt-loading can be described

Table 1
Projected MEA power densities, P_{MEA} (W/cm^2), and Pt-specific power densities, P_{Pt} (g_{Pt}/kW), for the possible polarization curves shown in Fig. 3

Assumptions	Catalyst activity	Cathode loading (mg_{Pt}/cm^2)	P_{MEA} at 0.65 V (W/cm^2)	P_{Pt} at 0.65 V (g_{Pt}/kW)
Current performance	Standard Pt/C	0.4	0.71	0.63
50% reduced η_{tx}	Standard Pt/C	0.4	0.91	0.48
50% reduced η_{tx}	Standard Pt/C	0.1	0.68	0.22
50% reduced η_{tx}	2× standard Pt/C	0.1	0.78	0.19
50% reduced η_{tx}	4× standard Pt/C	0.1	0.91	0.17

The assumed operating conditions are based on Fig. 1: H_2/air (s = 2/2) at 150 kPa_{abs} and T_{cell} = 80 °C (fully humidified) and the anode Pt-loading is assumed to be 0.05 mg_{Pt}/cm^2.

mathematically on the basis of the known O_2 reduction kinetics [8,10]:

$$\left.\frac{\partial E}{\partial \log[L_{ca}]}\right|_{p_{O_2},p_{H_2},T,i} = -b \quad (4)$$

where L_{ca} denotes the cathode Pt-loading. Eq. (4) states that the change in cell voltage with the logarithm of the cathode Pt-loading (assuming the same catalyst is used) is proportional to the Tafel-slope. Eq. (4), again, assumes that η_{tx} with H_2/air reactants is not changed by reducing the Pt-loading, which was shown to be the case for a two-fold loading reduction (from 0.4 to 0.2 mg_{Pt}/cm^2) for optimized MEAs [8], but has not yet been demonstrated for a reduction by a factor of 4 (i.e., down to 0.1 mg_{Pt}/cm^2). For a Tafel-slope of 70 mV/decade at 80 °C, a loading reduction by a factor of 2 or 4 is thus predicted to lead to a voltage loss across the entire current density range of ≈20 or ≈40 mV, respectively. This is depicted in Fig. 3, where the 50% η_{tx} reduced polarization curve (diamond symbols) is negatively shifted by ≈20 and ≈40 mV, reflecting a two- and four-fold Pt-loading reduction, respectively. Fig. 2 (open squares) shows that lowering the cathode Pt-loading from 0.4 to 0.1 mg_{Pt}/cm^2 indeed reduces the Pt-specific power density at 0.65 V to 0.22 g_{Pt}/kW, approaching very closely the automotive target of <0.2 g_{Pt}/kW. The drawback, however, is a simultaneous reduction of the MEA power density (see third row in Table 1) as well as a significant loss of voltage efficiency at all current densities (i.e., ca. −40 mV, see Fig. 3). Therefore, from an efficiency and cost (higher cost for bipolar plates, membranes, and diffusion media due to lower MEA power density) point of view, a lowering of the cathode Pt-loading to 0.1 mg_{Pt}/cm^2 using state-of-the-art Pt/C catalysts is not desirable, even though it would meet the g_{Pt}/kW requirement. The possible activity improvements of state-of-the-art Pt/C catalysts with a surface area of 75–90 m^2/g_{Pt} by further increasing the surface area (i.e., reducing the Pt-particle size) will be discussed in Section 3.2.3.

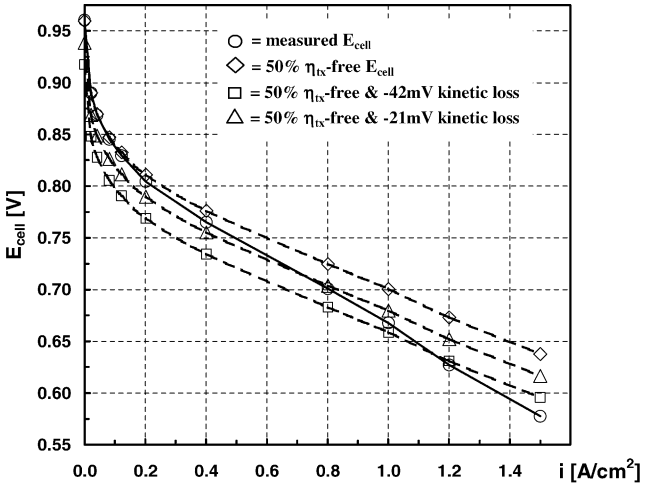

Fig. 3. (a) Circular symbols: original un-corrected polarization curve shown in Fig. 1a. (b) Diamond symbols: above polarization curve assuming a 50% reduced η_{tx} as shown in Fig. 1d. (c) Square symbols: above polarization curve assuming a 50% reduced η_{tx} and a four-fold lower Pt-loading (0.05/0.1 mg_{Pt}/cm^2), without catalyst improvement (i.e., E_{cell}-loss of 42 mV at all i's). (d) Triangular symbols: assuming a 50% reduced η_{tx} and a four-fold lower Pt-loading (0.05/0.1 mg_{Pt}/cm^2), with two-fold catalyst activity improvement (i.e., E_{cell}-loss of 21 mV at all i's).

A more viable approach is the implementation of higher mass activity Pt-alloy catalysts. As suggested by the literature and discussed in Section 4, the mass activity of Pt_xCo_{1-x}/C catalysts is approximately 2–4 times that of Pt/C [12,15], so that a lowering of the Pt-loading from 0.4 to 0.1 mg_{Pt}/cm^2 would result in a voltage loss of only ≈20 mV. Implementation of a cathode catalyst with a two-fold higher mass activity compared to Pt/C, would result in 0.19 g_{Pt}/kW at 0.65 V, while still achieving an MEA power density of 0.78 W/cm^2 (see fourth row of Table 1 and open triangles in Fig. 2). The most desired approach, however, would be the implementation of a Pt-alloy catalyst with a four-fold mass activity compared to Pt/C, which would enable to maintain an MEA power density of 0.91 W/cm^2 (see fifth row of Table 1 and star symbols in Fig. 2) at a cathode Pt-loading of 0.1 mg_{Pt}/cm^2. Currently, however, we have only been able to obtain a ca. two-fold enhancement over the mass activity of Pt/C (see Section 4), and further development of Pt-alloy catalysts is required to obtain the desired mass activity enhancement of a factor of 4. If this can be accomplished, a clear and viable path exists to meet both MEA power density and 0.2 g_{Pt}/kW targets for automotive PEMFC applications.

3.2. Specific and mass-specific activities of Pt catalysts

As was mentioned in Section 1, published activity data for Pt catalysts often vary by up to one order of magnitude, and clear benchmarks for the activity of Pt catalysts are needed in order to enable effective catalyst research. In the following sections, we will therefore present two different methodologies to determine the specific and the mass activities of Pt catalysts, developing benchmarking values for the activity of state-of-the-art Pt/C catalysts. While exchange current densities are the most fundamental intrinsic kinetic parameter, they can only be obtained by extrapolation of the measured currents over ca. four orders of magnitude, which inflicts large errors on the obtained values [10]. Therefore, activities in this manuscript will be evaluated at 0.9 V versus RHE, where data can be measured and no extrapolation is required.

3.2.1. Activities determined by 50 cm^2 H_2/O_2 fuel cell testing

Catalyst activity measurements of MEAs are generally evaluated using H_2/O_2 reactants in order to minimize mass-transport resistances [1,2,5,8,10,14,23,27–33]. While the interference from ohmic voltage loss contributions, ΔE_{ohmic}, can be excluded if in situ ohmic resistance measurements are available, mass-transport-induced voltage losses, η_{tx}, are more difficult to quantify and near-theoretical Tafel-slopes (i.e., 70 mV/decade at 80 °C) as well as high Pt-utilization in

Table 2
Catalyst characterization and catalytic performance characteristics of the four CCMs shown in Fig. 4

Catalysts	47% Pt/C (TKK)	46% Pt/C (TKK)	20% Pt/Vu (ETEK)	40% Pt/Vu (ETEK)
Anode/cathode (mg_{Pt}/cm^2)	0.4/0.4	0.50/0.51	0.15/0.17	0.37/0.38
$A_{Pt,MEA(ca)}$ (m^2/g_{Pt})	60	72	65	32
$A_{Pt,cat}$ (m^2/g_{Pt})	≈75	86 ± 7	71 ± 4	35 ± 2
u_{Pt} (%)	≈80	77–91	87–97	86–97
$i_{s(0.9\ V)}$ ($\mu A/cm^2_{Pt}$)	180	210	170	200
$i_{m(0.9\ V)}$ (A/mg_{Pt})	0.11	0.16	0.11	0.064

Specific Pt surface areas for the MEA cathodes (assuming 210 $\mu C/cm^2_{Pt}$) were determined using the driven-cell mode with humidified (50 °C dew points) H_2 (anode) and N_2 (cathode) at 0.5 slpm and 20 °C at a sweep rate of 20 mV/s. MEA catalyst utilization, u_{Pt}, is defined as the ratio of the MEA cathodes' specific Pt surface area ($A_{Pt,MEA(ca)}$) to that of the catalyst ($A_{Pt,cat}$ including the standard deviation from five independent experiments at room temperature in aqueous electrolyte). Specific activities, $i_{s(0.9\ V)}$, and mass activities, $i_{m(0.9\ V)}$, determined at 0.9 V and 80 °C at an O_2 partial pressure of 100 kPa_{abs}.

the MEA, u_{Pt}, are necessary but not always sufficient conditions to ascertain the absence of mass-transport losses even at low current densities. The latter is probably one of the major causes for the observed discrepancies in reported O_2 reduction activities of Pt catalysts, varying by up to one order of magnitude. The reason lies in the fact that state-of-the-art MEAs which exhibit zero mass-transport resistance in H_2/O_2 fuel cell testing are generally prepared according to proprietary procedures using commercially non-available diffusion media, membranes, and ionomers. Thus, Fig. 4 shows (grey circles) that the MEA used in Fig. 1 (circular symbols) yields perfectly straight Tafel-lines with a slope of 70 mV/decade in a plot of the *iR*-free voltage, $E_{iR\text{-free}}$, versus the logarithm of the H_2-crossover corrected current density, i_{eff}, and exhibits a catalyst utilization of the MEA of ca. 80% (Table 2, second column). Using the effective current density at 0.9 V (44 mA/cm^2, see Fig. 4), the cathode Pt-surface area obtained in the MEA, $A_{Pt,MEA(ca)}$, and the Pt-loading, it is straightforward to determine the mass-activity,

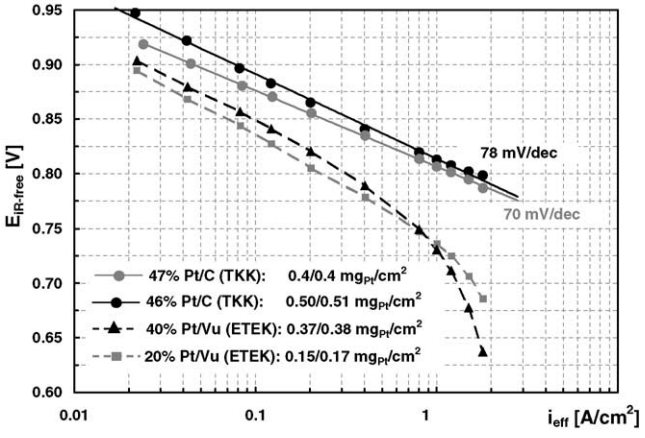

Fig. 4. Resistance-corrected 50 cm^2 H_2/O_2 performance of both the CCM described and shown in Fig. 1 (grey circles) as well as three Nafion-112® based CCMs (see Section 2.1.2). Measurements were taken at T_{cell} = 80 °C with fully humidified (80 °C dew points) reactants at 150 kPa_{abs} (H_2/O_2 stoichiometric flows of s = 2/9.5 for $i \geq 0.2$ and 0.2 A/cm^2 flows for $i <$ 0.2 A/cm^2). Voltages were averaged between 10 and 15 min holding time at each current density. The resistance-corrected cell voltage, $E_{iR\text{-free}}$, was determined via on-line high-frequency resistance measurements (evaluated at 1 kHz) vs. current density. Current densities were H_2 crossover corrected to yield the shown effective current density, i_{eff}.

$i_{m(0.9\ V)}$, of 0.11 A/mg_{Pt} and the specific activity, $i_{s(0.9\ V)}$, of 180 $\mu A/cm^2_{Pt}$. Unfortunately, such purely kinetically controlled H_2/O_2 polarization curves are not always obtained with non-optimized MEAs and diffusion media (see, e.g., Fig. 5 in Ref. [34]), in which case the mass-transport-induced losses cannot be quantified and, consequently, the determination of Pt catalyst activities is unreliable.

Quite clearly, more reliable testing methods need to be developed to support the effective development of new cathode catalysts in different laboratories. This is the reason why we propose a preparation method for CCMs which is based solely on commercially available components (see Section 2.1.2) and which produce kinetically controlled H_2/O_2 performance curves with near-theoretical Tafel-slopes, at least at low current densities [23]. It should be noted, however, that no attempt was made to optimize the CCM preparation such that state-of-the-art H_2/air performance as shown in Fig. 1 can necessarily be obtained. In order to determine the viability of this approach, we tested three different catalysts listed in Table 2 (last three columns). The resulting H_2/O_2 polarization curves are shown in Fig. 4, demonstrating that near-theoretical kinetically controlled Tafel-slopes are obtained for all three catalysts at <0.2 A/cm^2. Similarly, Table 2 shows that the Pt utilization in the MEA, u_{Pt}, is on the order of 80–90%. Both observations are necessary conditions for obtaining reliable catalyst activities. The extracted values for $i_{s(0.9\ V)}$ (170–210 $\mu A/cm^2_{Pt}$, see Table 2) agree closely with the values obtained for a state-of-the-art CCM (second column in Table 2); on the other hand, the values for $i_{m(0.9\ V)}$ reflect the differences in Pt-surface area, so that the 40% Pt/Vulcan ETEK catalyst exhibits only about half of the mass activity obtained with the other three catalysts (it should be noted that this catalyst no longer represents the current state of development of high-wt.% ETEK catalysts). While we have only tested three catalysts with this CCM preparation method based on commercially available materials, the method clearly enables one to distinguish two-fold differences in mass activity, produces consistent results, and seems appropriate for testing new catalysts in laboratories where no other improved components are available.

Reviewing the activities (at 0.9 V and 80 °C at 100 kPa_{abs} O_2 partial pressure) and catalyst surface areas for the various

catalysts listed in Table 2, the following conclusions may be drawn: (i) the highest Pt surface area, $A_{Pt,cat}$, for a high-wt.% Pt/C catalysts (46% Pt/C from TKK) is ca. 86 ± 7 m^2/g_{Pt}, reflecting a significant increase over older catalyst preparation technology (40% Pt/Vulcan from ETEK), (ii) specific activities, $i_{s(0.9\ V)}$, for all the examined catalysts are ca. 200 $\mu A/cm^2_{Pt}$, indicating a negligible particle size effect in this narrow range of particle size (i.e., ca. 2–4 nm), and, consequently, (iii) the highest mass activity, $i_{m(0.9\ V)}$, of 0.16 A/mg_{Pt} is obtained for the catalyst with the highest Pt surface area. It should be noticed that the catalyst used in the state-of-the-art CCM (47% Pt/C from TKK) is not the catalyst with the highest mass activity (46% Pt/C from TKK), which has to do with the fact that the optimization of a CCM's H_2/air performance very much depends on the morphology of the carbon support, requiring an unfortunately cumbersome optimization process. Since the performance targets shown in Figs. 1 and 2 were based on the 47% Pt/C (TKK) catalyst, the required improvement in mass activity of a factor of 4 implies that the desired four-fold mass activity of an optimized Pt-alloy corresponds to a mass activity of $i_{m(0.9\ V)} \approx 0.45\ A/mg_{Pt}$ and to a specific activity of $i_{s(0.9\ V)} \approx 800\ \mu A/cm^2_{Pt}$ (assuming the same Pt surface area).

Finally, the activities listed in Table 2 may be compared to activities published in the literature (Table 3), whereby a first-order p_{O_2} dependence on the activity at 0.9 V is assumed [10] in order to normalize mass and specific activities to 100 kPa_{abs} O_2, expressed as $i^*_{m(0.9\,V)}$ and $i^*_{s(0.9\,V)}$, respectively (no correction was applied to normalize the H_2 partial pressure to 100 kPa_{abs}, neglecting the p_{H_2} effect on the reversible potential, which otherwise would lead to slightly lower normalized activities as is explained in Section 4.1.3). A comparison of the activities for Pt/C catalysts with state-of-the-art surface areas of >60 m^2/g_{Pt} ($i_{s(0.9\ V)} \approx$ 170–210 $\mu A/cm^2_{Pt}$ and $i_{m(0.9\ V)} \approx$ 0.11–0.16 A/mg_{Pt}, see Table 2) with literature data agrees within a factor of 1.5 with several published activities (see first to seventh rows in Table 3), an acceptable range considering the different testing conditions. While the specific activities, $i^*_{s(0.9\,V)}$, are consistent for a larger range of literature reports (including rows 8–12 in Table 3), the reported mass activities, $i^*_{m(0.9\,V)}$, are significantly lower, which can be explained by the lower Pt surface areas in these MEAs, $A_{Pt,MEA(ca)}$ (see Table 3). Therefore, for the most stringent comparison of the activities of different catalysts, accurate assessment of both Pt surface areas in the MEA and specific activities are required to yield reliable results. Nevertheless, several literature reports show a factor of 5–10 lower values of $i^*_{m(0.9\,V)}$ and $i^*_{s(0.9\,V)}$ (see rows 13–15 in Table 3), demonstrating that the quantification of catalyst activity in H_2/O_2 MEA testing can be fraught with significant errors if non-optimized MEAs are used which exhibit mass-transport-related losses even at the low current densities at 0.9 V. Since the presence of these losses is not always clear from the experimental data, it is therefore imperative that the experimental methods (i.e., testing procedure and MEA preparation) are verified by determining whether the correct activities can be obtained for standard Pt/C catalysts, prior to testing new and unknown catalysts.

Table 3
Comparison of mass activities, $i^*_{m(0.9\,V)}$, and specific activities, $i^*_{s(0.9\,V)}$, at 0.9 V and normalized (assuming first order with respect to p_{O_2}) to an O_2 partial pressure of 100 kPa_{abs}

Catalyst	$L_{cathode}$ (mg_{Pt}/cm^2)	Membrane	T_{cell} (°C)	p_{cell} (kPa_{abs})	p_{O_2}[a] (kPa_{abs})	$A_{Pt,MEA(ca)}$ (m^2/g_{Pt})	$i^*_{m(0.90\,V)}$ (A/mg_{Pt})	$i^*_{s(0.90\,V)}$ ($\mu A/cm^2_{Pt}$)	Reference
Not specified	0.40	Not specified	65	100	75	60	0.20	330	[1]
46% Pt/C (TKK)	0.51	Nafion-112®	80	150	103	72	0.16	210	Table 2
20% Pt/Vu (ETEK)	0.40	Nafion-115®	70	200	169	29	0.13[b]	470[b]	[32]
20% Pt/Vu (ETEK)	0.17	Nafion-112®	80	150	103	65	0.11	170	Table 2
47% Pt/C (TKK)	0.40	≈900EW/25 μm	80	150	103	60	0.11	180	Table 2
40% Pt/Vu (JM)	0.44	Nafion-115®	80	308	261	55	0.10	190	[27]
47% Pt/Vu (TKK)	0.15–0.40	Nafion-112®	80	270	223	52	0.10	190	[10]
50% Pt/C (TKK)	0.25	Nafion-112®	80	100	100	62[c]	0.07	110[c]	[33]
40% Pt/Vu (ETEK)	0.38	Nafion-112®	80	150	103	32	0.064	200	Table 2
20% Pt/Vu (ETEK)	0.30	Dow[d]	80	137	90	20	0.056	310	[30]
40% Pt/Vu	0.40	Nafion-117®	80	500	453	19	0.033	170	[29]
20% Pt/Vu	0.40	Nafion-117®	80	500	453	13	0.028	210	[29]
20% Pt/Vu (JM)	0.61	Dow[d]	80	300	253	71	0.029	40	[24]
20% Pt/Vu (JM)	0.50	Dow[d]	75	377	340	26	0.010	37	[14]
20%Pt/Vu	0.35	Nafion-117®	70	100	69	35	0.013	36	[31]

All data were acquired in PEM single cells using fully humidified (one noted exception) H_2/O_2 reactants (stoichiometric feed rates of $s \geq 10/10$ (H_2/O_2) at 0.90 V).

[a] Hydrogen and oxygen partial pressures were calculated assuming 100% relative humidity (i.e., $p_{O_2} = p_{ca} - p_{H_2O,sat}$).

[b] Data were extracted from the $E_{iR\text{-free}}$ vs. i plot for the best electrode with 1.9 mg_{Nafion}/cm^2 (Fig. 3 in this reference).

[c] $A_{Pt,CCM(ca)}$ was not given and the CO chemisorption value of the catalyst is used instead.

[d] The membrane product number of the Dow-membrane was: XUS-13204.10.

3.2.2. Rotating disk electrode measurements of high-surface-area catalysts

An alternative methodology for determining both $i^*_{m(0.9\,V)}$ and $i^*_{s(0.9\,V)}$ of high-surface-area catalysts is the thin-film rotating disk method (TF-RDE) [12,13,25,35]. We will show in the following that the TF-RDE method not only produces the same activity ranking for different Pt/C catalysts as was observed for H_2/O_2 MEA testing (Table 2), but also results in a quantitative agreement within a factor of 2 *if* measurements are taken at comparable temperatures (60 °C) in non-adsorbing 0.1 M $HClO_4$ electrolyte. This agreement is quite reasonable, considering the different nature of the electrolytes (i.e., PFSA ionomers versus aqueous $HClO_4$). In order to conduct quantitative measurements, however, the amount of catalyst dispersed onto the glassy-carbon disk electrode must be known precisely, while at the same time very low loadings (on the order of $\ll$100 $\mu g_{catalyst}/cm^2$) need to be applied in order to avoid excessive mass-transport losses in overly thick (i.e., >1 μm) catalyst agglomerates deposited on the disk electrode [13]. If thicker catalyst agglomerates (typically catalyst with PFSA ionomers as binders) are used [36–38]. the mass-transport characteristics of a rotating disk electrode are not satisfied anymore, and mathematical models with many unknown parameters [37,38] (e.g., agglomerate structure, diffusivities in ionomer films, etc.) must be used to quantify catalyst activity, introducing a large uncertainty in the measured activities (for a more detailed discussion, see Ref. [13]). Therefore, in the following described TF-RDE experiments, loadings of $\ll$100 $\mu g_{catalyst}/cm^2$ at ionomer/carbon ratios of <1/1 were used, resulting in catalyst agglomerate thicknesses of <1 μm (assuming 50% void volume of the deposited agglomerates and an ionomer and carbon density of ca. 2 g/cm^3), i.e., approximately one order of magnitude thinner than the mass-transport boundary layer of an RDE in the O_2 reduction activity measurements at 1600 rpm conducted in this study [39].

Fig. 5 shows an example of the O_2-reduction current densities obtained in 0.1 M $HClO_4$ at 60 °C and 1600 rpm, using a 20 wt.% Pt/Vulcan (ETEK) catalyst at a loading of 14.3 $\mu g_{Pt}/cm^2$. The diffusion-limited current density of ca. 6 mA/cm^2 is in excellent agreement with data obtained on a smooth polycrystalline Pt-disk electrode under the same experimental conditions (see Fig. 6b in Ref. [40]), demonstrating the negligible mass-transport effects imposed by the ionomer-binder used to ''glue'' the catalysts to the glassy-carbon disk [13,35]. While the lower sweep rate of 5 mV/s offers less interference from capacitive currents (<4% at 0.9 V), lower activities corresponding to a 10–15 mV negative potential shift compared to the activities obtained at 20 mV/s are observed. Part of this lower activity at 5 mV/s is most likely due to the hysteresis in the adsorption of oxygen-containing species on Pt (often referred to as OH_{ads}) and their negative impact on the O_2-reduction activity [41–43], thereby leading to lower activities at lower sweep rates (a similar phenomenon is observed in PEMFCs, where activities at 0.9 V show a significant initial time decay, presumably due to slow Pt-oxide formation [44]). Part of it, however, may also be due to electrode contamination in RDE experiments at low sweep rates, produced by trace impurities in the large excess of electrolyte compared to the Pt surface area, a problem which becomes more pronounced when electrodes with very low roughness factors (rf = ratio of Pt surface area to geometric disk surface area) are used (e.g., smooth polycrystalline disk electrodes with rf ≈ 1). The latter trace impurity-related effects become apparent when subsequent sweeps at 5 mV/s do not superimpose and/or when diffusion-limited currents begin to depend on the sweep rate, both of which is not the case for the measurements in Fig. 5.

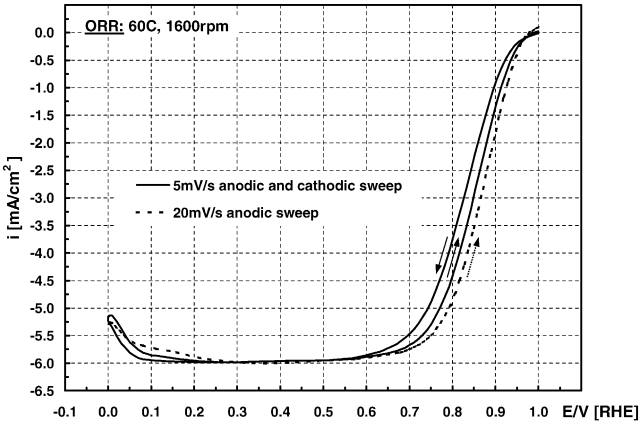

Fig. 5. Oxygen reduction current densities on 20% Pt/Vulcan (14.3 $\mu g_{Pt}/cm^2$) supported on a glassy-carbon disk electrode at 1600 rpm in 0.1 M $HClO_4$ at 60 °C: sweeps at 5 mV/s (solid line) and 20 mV/s (dashed line; positive-going sweep only). All potentials are referred to the reversible hydrogen electrode under the same conditions.

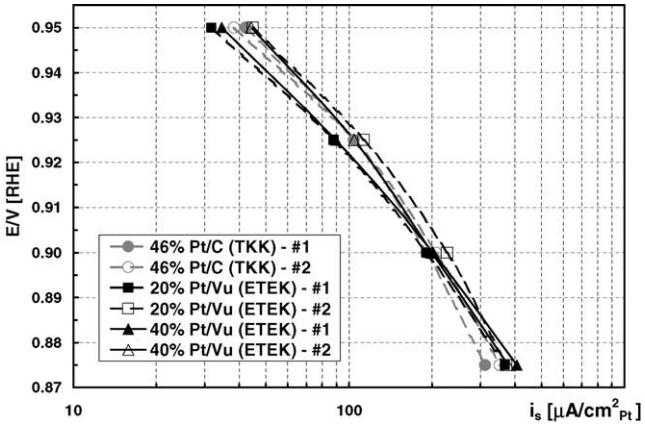

Fig. 6. Specific activities, i_s, for the ORR at 60 °C on Pt/C catalysts (two repeats each) supported on glassy-carbon disk electrodes (Pt-loadings ranging from 12.7 to 14.3 $\mu g_{Pt}/cm^2$). Data are shown for the positive-going sweep at 5 mV/s going from 0 to 1.0 V (RHE) in O_2-saturated 0.1 M $HClO_4$ at 1600 rpm. Potentials are referred to the reversible hydrogen electrode under the same conditions.

Fig. 6 shows the specific activities of three different catalysts (two repeats each) at 5 mV/s in 0.1 M $HClO_4$ at 60 °C, calculated from the experimental data using the well-known mass-transport correction for rotating disk electrodes [13]:

$$i_k = \frac{i_d i}{i_d - i} \quad (5)$$

where i is the experimentally obtained current, i_d refers to the measured diffusion-limited current, and i_k the mass-transport free kinetic current. Specific activities can be determined via calculation of i_k using Eq. (5) and normalization with the Pt surface area, $A_{Pt,cat}$, and the Pt loading (both listed in Table 2) [10]. Quite clearly, the specific activity at 0.9 V of all three catalysts is centered about 200 $\mu A/cm^2_{Pt}$, in excellent agreement with the H_2/O_2 MEA data for the same catalysts listed in Table 2 (last three columns from the right). While close to theoretical Tafel-slopes (i.e., 65 mV/dec at 60 °C) are obtained at potentials between 0.95 and 0.875 V, higher Tafel-slopes are observed at lower potentials (not shown). This change in slope indicates the growing inaccuracy of the RDE mass-transport corrections as the current density approaches the diffusion-limited current density (this occurs somewhat earlier in the less ideal case of a TF-RDE configuration compared to a smooth Pt-disk RDE), and activities are best extracted at current density values below $i_d/2$, where mass-transport corrections according to Eq. (5) are less than a factor of 2. This requirement is met at 0.9 V for all the catalysts tested in this study. This is the reason why the choice of 0.9 V as a benchmark for catalyst activity should be considered *good practice* for both TF-RDE measurements as well as for H_2/O_2 MEA measurements, as in either case interferences from mass-transport-induced losses cannot be unambiguously excluded at the higher current densities observed below 0.9 V.

From the same experimental data, one can also determine the mass activities of the catalysts via calculation of i_k (Eq. (5)) and normalization to the Pt-loading. At 0.9 V, the mass activities of the 46% Pt/C (TKK) and the 20% Pt/Vulcan (ETEK) catalyst are essentially identical (Fig. 7), while the mass activity for the 40% Pt/Vulcan (ETEK) catalyst is clearly a factor of 2 lower. This is not only consistent with the H_2/O_2 MEA data (Table 2), but also is in practically quantitative agreement as can be seen by comparing the bold-faced entrees in Table 4 (second to last column) with those in Table 2. While few data in the literature are published under the same conditions, the last row in Table 4 lists recent literature data under the same conditions on the 20% Pt/Vulcan (ETEK) catalyst [12], showing excellent agreement with the same catalyst used in our study.

In summary, the benchmark activities for carbon-supported Pt catalysts determined by either H_2/O_2 MEA testing at 80 °C or TF-RDE measurements at 60 °C is in rather good quantitative agreement. For the state-of-the-art 46% Pt/C catalyst, either method yields a specific activity of

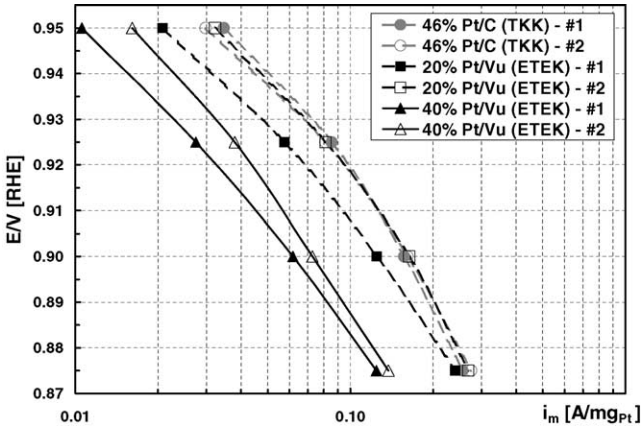

Fig. 7. Mass activities, i_m, for the ORR at 60 °C on Pt/C catalysts (two repeats each) supported on glassy-carbon disk electrodes (Pt-loadings ranging from 12.7 to 14.3 $\mu g_{Pt}/cm^2$). Data are shown for the positive-going sweep at 5 mV/s going from 0 to 1.0 V (RHE) in O_2-saturated 0.1 M $HClO_4$ at 1600 rpm. Potentials are referred to the reversible hydrogen electrode under the same conditions.

≈200 $\mu A/cm^2_{Pt}$ and a mass activity of 0.16 A/mg_{Pt}. In light of the slightly different temperatures this may be somewhat counter-intuitive, but can probably be ascribed to the different time-scales of the experiments (15 min/point for MEA testing versus 5 mV/s for TF-RDE measurements), compensating the effect of a higher temperature in MEA measurements with the effect of slightly reduced activities at the extended measurement time at a given potential [44]. To investigate the influence of temperature and the time-scale effect further, H_2/O_2 MEA testing is underway [23]. Nevertheless, excellent quantitative comparison between different catalysts can be obtained by both methods.

3.2.3. Pt-particle size effect observed in RDE measurements

In order to comprehend the possibility of enhancing the mass activity of the state-of-the-art 46% Pt/C catalysts by increasing its Pt surface area beyond 87 m^2/g_{Pt}, it is important to determine whether so-called *Pt-particle size effects* on the O_2-reduction activity play a role in non-adsorbing electrolytes (i.e., PFSA ionomers and $HClO_4$). The Pt-particle size effect is well understood in the context of phosphoric acid fuel cells (PAFCs) and describes the observation that the specific activity of Pt in phosphoric acid decreases by a factor of ≈3 as the Pt-particle size decreases from 12 to 2.5 nm, while the mass activity shows a maximum at ≈3 nm [45], consistent with other reports in the PAFC literature [14,46]. This effect is generally ascribed to the impeding effect of specific anion adsorption on different crystal faces, the distribution of which changes with Pt-particle size [46]. It is less clear, whether a Pt-particle size effect also exits in non-adsorbing electrolytes (i.e., in the PEMFC environment), even though recent data in 0.1 M $HClO_4$ [14] suggest that a similar variation in specific activity as well as a mass activity maximum at ca. 3–4 nm

Table 4
Specific activities, $i_{s(0.9\ V)}$, and mass activities, $i_{m(0.9\ V)}$, for the ORR at 0.90 V and 60 °C determined from positive-going sweeps at 20 and 5 mV/s from 0 to 1.0 V (RHE)

	L_{Pt} ($\mu g_{Pt}/cm^2$)	$A_{Pt,cat}$ (m^2/g_{Pt})	$i_{s(0.9\ V),20\ mV/s}$ ($\mu A/cm^2_{Pt}$)	$i_{s(0.9\ V),5\ mV/s}$ ($\mu A/cm^2_{Pt}$)	$i_{m(0.9\ V),20\ mV/s}$ (A/mg_{Pt})	$i_{m(0.9\ V),5\ mV/s}$ (A/mg_{Pt})	Reference
5 mm Ptpc-disk	n.a.	rf = 1.13[a]	2770	1710	n.a.	n.a.	Data not shown
5 mm Ptpc-disk	n.a.	rf = 1.17[a]	2460	1020	n.a.	n.a.	Data not shown
Pt-black (HiSpec1000, JM)	43.5	5.9	860	720	0.050	0.042	Data not shown
Pt-black (HiSpec1000, JM)	43.5	4.9	840	620	0.041	0.030	Data not shown
40% Pt/Vu (ETEK)	**13.7**	**36**	**310**	**190**	**0.11**	**0.069**	Figs. 6 and 7
40% Pt/Vu (ETEK)	**13.7**	**31**	**320**	**200**	**0.098**	**0.062**	Figs. 6 and 7
20% Pt/Vu (ETEK)	**14.3**	**72**	**260**	**230**	**0.19**	**0.16**	Figs. 6 and 7
20% Pt/Vu (ETEK)	**14.3**	**65**	**300**	**200**	**0.20**	**0.13**	Figs. 6 and 7
45.9% Pt/HSC-E (TKK)	**12.7**	**82**	**240**	**190**	**0.20**	**0.16**	Figs. 6 and 7
45.9% Pt/HSC-E (TKK)	**12.7**	**78**	**290**	**210**	**0.22**	**0.16**	Figs. 6 and 7
46.5% Pt/HSC-E (TKK)	16.2	79	250	220	0.20	0.17	Data not shown
27% Pt/Ketjen (in-house)	16.1	120	160	150	0.20	0.18	Data not shown
20% Pt/Vu (ETEK)	14	66	–	210	–	0.16	[12]

Catalysts were supported on glassy-carbon disk electrodes (for Pt-loadings see below) and rotated at 1600 rpm in O_2-saturated 0.1 M $HClO_4$. No correction was made for the contribution of capacitive currents, estimated to be below 4% (15%) at 5 mV/s (20 mV/s) and 0.90 V. Pt surface areas were determined via cyclic voltammetry (both hydrogen adsorption and desorption) in the same electrolyte at 25 °C and 20 mV/s.
[a] The ratio of Pt surface area to geometric disk area.

Pt-particle size might occur. It is suggested [14,47] that this is due to Pt-particle size induced changes in the potential-dependent adsorption of oxygen-containing species, OH_{ads}, which are frequently believed to reduce the O_2-reduction activity [42,43].

All the Pt catalysts shown in Table 2 displayed Pt surface areas of 35–87 m^2/g_{Pt} ($A_{Pt,cat}$ in Table 2), corresponding to a difference in Pt-particle size by a factor of only 2.5, based on the fact that the Pt surface area is approximately inversely proportional to the Pt-particle size, d_{Pt}. While the Pt-particle size for the catalysts in Table 2 was not determined in this study, high-resolution transmission electron spectroscopy on the 20% Pt/Vulcan (ETEK) catalyst yielded an average Pt-particle size of 3.4 nm [12], suggesting that the average Pt-particle sizes for the 46% Pt/C (TKK) catalyst and the 40% Pt/Vulcan (ETEK) catalyst equate to approximately 2.8 and 6.9 nm, respectively (again assuming $d_{Pt} \propto 1/[m^2/g_{Pt}]$). Therefore, if the data in Ref. [14] were correct, the mass activity of the state-of-the-art 46% Pt/C (TKK) catalyst with its 86 ± 7 m^2/g_{Pt} surface area would not be expected to increase with further Pt-dispersion, since its Pt-particle size falls near the expected range of maximum mass activity.

In order to test this hypothesis, we conducted RDE and TF-RDE measurements in 0.1 M $HClO_4$ (60 °C) on Pt catalysts with largely varying Pt-particle sizes, ranging from smooth polycrystalline Pt (d_{Pt} on the order of hundreds of nm) to Pt-black (d_{Pt} on the order of 10–20 nm) to a very high-surface-area 27% Pt/C catalyst with $d_{Pt} \approx 2$ nm (120 m^2/g_{Pt}). These experiments are most meaningful at a sweep rate of 20 mV/s, since large experimental scatter is observed for the smooth polycrystalline Pt-disk at 5 mV/s (see first and second row in Table 4) due to the above-mentioned trace impurity issue at low sweep rates with low-surface-area electrodes. The resulting specific activities as a

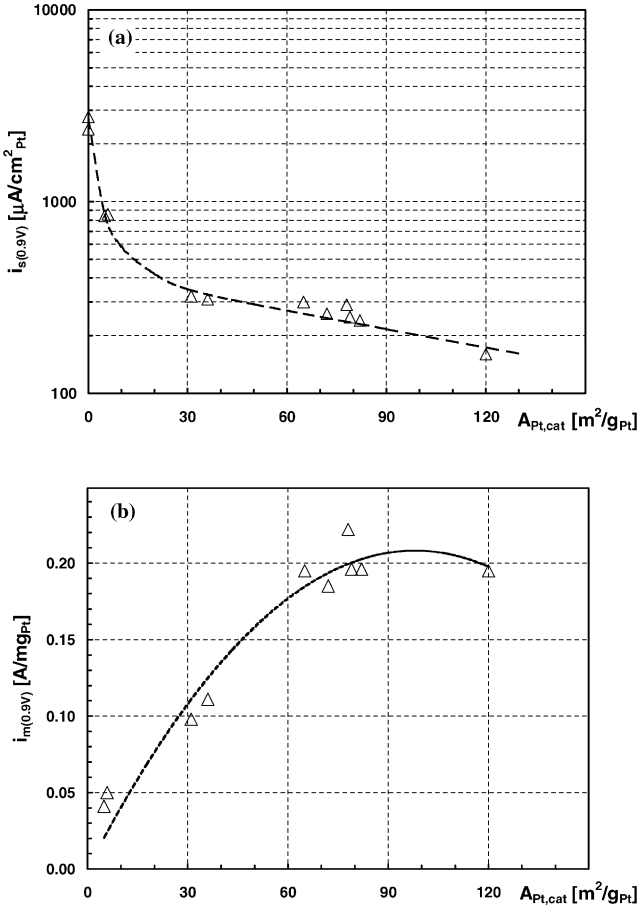

Fig. 8. ORR activities of polycrystalline Pt (shown at "0 m^2/g_{Pt}"), Pt-black (data at ca. 5 m^2/g_{Pt}), and Pt/C catalysts at 0.9 V and 60 °C determined via RDE-measurements in O_2-saturated 0.1 M $HClO_4$. Activities were obtained from positive-going sweeps at 20 mV/s, going from 0 to 1.0 V (RHE). (a) Specific activities, $i_{s(0.9V)}$; (b) mass activities, $i_{m(0.9\ V)}$. No correction was made for the contribution of capacitive currents, estimated to be below 15% under these conditions.

function of Pt surface area are shown in Fig. 8a, demonstrating that a more than one order of magnitude variation in specific activity is obtained between these different catalysts! While the absolute activities are by a factor of 10 higher than the ones reported in Ref. [14], the ratio of specific activities between 5 and 120 m^2/g_{Pt} is indeed quite comparable. Similarly, as shown in Fig. 8b, the mass activities go through a shallow maximum somewhere between 70 and 120 m^2/g_{Pt} (for further details, see Table 4).

While the Pt-particle size effect in non-adsorbing 0.1 M $HClO_4$ (and by analogy in the PEMFC environment) is quite apparent from Fig. 8, its cause is still unclear. If the hypothesis of an increasing adsorption strength of OH_{ads}-species together with their negative impact on the O_2-reduction reaction with decreasing Pt-particle size were true, the one order of magnitude difference in specific activity between polycrystalline Pt and the 46% Pt/C (TKK) catalyst (see Table 4) would imply a negative shift of the oxide adsorption/desorption potential in the cyclic voltammograms by approximately 65 mV (based on a Tafel-slope of 65 mV/dec in conjunction with Eq. (4)). Fig. 9 shows that this is indeed the case: the oxide adsorption/desorption wave of the 46% Pt/C (TKK) catalyst occurs ca. 80 mV negative compared that on polycrystalline Pt, while that on the Pt-black catalyst falls in between. While this may not be a definitive proof for the role of site-blocking OH_{ads}-species in the O_2 reduction reaction [41–43,47], it certainly does substantiate this hypothesis.

Considering the excellent agreement so far observed between the activities measured by TF-RDE in 0.1 M $HClO_4$ and by H_2/O_2 MEA testing, it is quite reasonable to predict that the same Pt-particle size effects as shown in Fig. 8b would occur in PEMFCs. This in turn implies that little or no gain in mass activity is anticipated for Pt/C catalysts with surface areas in excess of ≈90 m^2/g_{Pt}, and that the development of more active Pt-alloys (or of yet unknown non-Pt catalysts) is the only viable path to reach the required mass activity of 0.45 A/mg_{Pt} (i.e., a factor of ≈3 over the state-of-the-art 46% Pt/C catalyst).

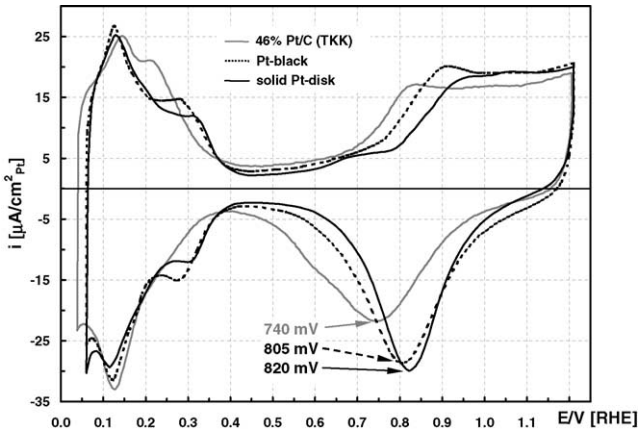

Fig. 9. Cyclic voltammograms of carbon-supported Pt, Pt-black, and polycrystalline Pt in terms of Pt-surface area normalized current densities ($\mu A/cm^2_{Pt}$). Data were recorded in 0.1 M $HClO_4$ at 25 °C and 20 mV/s.

4. Pt-alloy catalysts for PEMFCs

Significant overpotentials (η_{ORR} of the order of ∼400 mV at 1.5 A cm^{-2}) exist for the ORR as mentioned in the previous section and depicted in Fig. 1. Currently, state-of-the-art MEAs are typically composed of highly dispersed Pt on carbon support, often at high-wt.% Pt (in the range 40–50% Pt) that ensures the formation of thin catalyst layers of 10–15 μm (Pt-loading = 0.40 mg/cm^2). The specific activity (i_s) of Pt supported on moderate to high-surface-area carbon catalysts at 80 °C under O_2 at a partial pressure of ∼100 kPa_{abs} at 0.90 V is ∼180–210 $\mu A/cm^2_{Pt}$, and the mass activity (i_m) ∼0.11–0.16 A/mg_{Pt} (see Table 2). To meet projected cost targets for automotive PEMFC commercialization, it is essential to reduce the Pt-loading to ca. 1/4 of the current state-of-the-art MEA cathode catalyst layer, i.e., from about 0.40 to 0.10 mg/cm^2 without a loss in cell voltage, while maintaining maximum power density and cell efficiency. Thus, it will be necessary to raise the activity of Pt or a modified Pt-alloy catalyst four-fold. Alternately, an inexpensive non-noble metal catalyst might also provide a solution to lower costs as discussed in the next section. It should be noted that it would be necessary to maintain the enhanced catalytic activity over ∼5000 h or more for automotive applications with low degradation rates of a few μV/h.

One of the pathways to achieve the lower η_{ORR} is through the modification of the intrinsic catalytic activity of Pt surface atoms by alloying the catalyst with base-metal that results in the formation of bimetallic surfaces. There have been several attempts made to hypothesize or at least draw strong correlations between the enhanced activity of Pt-alloys over Pt that may be broadly classified as structural factors, inhibition by anion adsorption, electronic factors, and surface sensitive factors [45]: (i) crystalline Pt has an FCC lattice with a lattice parameter of 3.93 Å as measured from XRD measurements. It has been observed that the base-metal elements smaller than Pt, when alloyed with Pt, enter the crystal structure through substitution and cause a lattice contraction. The increasing electrocatalytic activity of the Pt-alloys (such as PtCr, PtV, PtTi, PtW, PtAl, PtAg) show a strong correlation with a decrease in interatomic or nearest-neighbor distance between Pt atoms [48]. This effect has been attributed to the smaller Pt–Pt bond distances resulting in more favorable sites that enhance the dissociative adsorption of oxygen. (ii) A second hypothesis is related to structure-sensitive inhibiting effect of OH_{ads} in perchloric acid as well as sulfate/bisulfate anion adsorption in sulfuric acid: It is well known that in high-surface-area Pt/C dispersed catalysts, the dominant Pt crystal faces that are exposed are ⟨1 1 1⟩ and ⟨1 0 0⟩. Based on RDE measurements of the ORR on Pt(*h k l*) in liquid electrolytes it is

known that the ⟨1 1 1⟩, ⟨1 0 0⟩, ⟨1 1 0⟩ surfaces are increasingly active in that order for sulfuric acid [49] and ⟨1 0 0⟩, ⟨1 1 0⟩, ⟨1 1 1⟩ in perchloric acid [41]. Other studies [40] showed that Pt_3Co-alloys have activities that are several times that of polycrystalline Pt which was attributed to the inhibition of OH_{ad} formation on the Pt in the alloys. (iii) Yet other studies [50] suggest that surface roughening of the Pt-alloy takes place due to dissolution or leaching of the more easily oxidizable base-metal in bulk alloys leading to higher activity via surface area increase. (iv) Electronic factors associated with d-band vacancies are also expected to play and important role. Several studies [51,52] have been conducted showing that alloying of Pt with transition metal elements increased the Pt d-band vacancy and decreased the Pt–Pt bond distance depending on the electro-negativity of the transition metal. XANES data demonstrated that the OH_{ads} onset which is at 0.80 V for Pt/C shifted to more positive potentials in some Pt-alloys. (v) Also discussed in the literature [40,53] are the replacement of buried atoms of Pt or surface-enriched Pt-skin or skeletal structures (where Pt and base-metal are exchanged in the surface layers) that lead to high-activity enhancements due to weaker Pt-OH_{ads} in the electronically modified Pt skin.

Despite our lack of a complete understanding of the mechanisms for the enhancement of Pt-alloys over Pt, the use of Pt-alloys/C has already been demonstrated in practical PAFC applications to produce 20–40 mV gains in activity as well as improved lifetime exceeding 40,000 h [46]. We shall therefore briefly review the PAFC, RDE, and PEMFC literature related to Pt-alloy electrocatalysts, and discuss the issues specifically related to using Pt-alloy catalysts in PEMFC with the help of some experimental data on ex situ alloy leaching, cell performance, and durability.

4.1. Literature review

4.1.1. Alloy catalysts in phosphoric acid fuel cells (PAFCs)

UTC (known at different times as United Aircraft, Pratt and Whitney, and International Fuel Cells) originally developed some of the first carbon-supported Pt electrocatalysts in the 1970s to increase the rate of the electrode reaction and lower the total catalyst loading from 5 mg/cm^2 for Pt-black to less than 1 mg/cm^2 for Pt/C. An excellent review of the breadth and depth of PAFC catalysis research and development carried out at UTC can be referred to in an article by Landsman and Luczak [46]. This not only lowered the cost but also improved the durability of the PAFC electrodes. Having maximized the utilization and activity in gas diffusion electrodes made from Pt/C catalysts sintered with PTFE, the next logical step (in the 1980s) was to attempt to enhance the intrinsic activity of Pt by altering its structural properties. One of the proposals for the rate-determining step in the ORR was hypothesized to be the dissociation of the O–O bond in the initially formed peroxyl radical: it seemed then that by changing the spacing between the Pt–Pt atoms, the strength of the Pt–O adsorption could be strengthened or weakened favorably and it was attempted by alloying Pt with transition metals. Thus, a procedure was developed to form high surface Pt-alloys that involved mixing a pre-formed Pt/C catalyst with the oxide of a chosen base-metal followed by heat treatment to 800–1000 °C in an inert atmosphere [54]. The process called *carbothermal reduction* results in part of the carbon support being consumed in the reduction of the metal oxide to metal which subsequently reacts with Pt to form Pt-alloy. Serious effort was put into the development of Pt-alloys starting with binaries such as PtV/C and culminating in ternaries such as PtCoCr/C, PtRhFe/C, and PtIrCr/C. The mass activity of the Pt-alloys were 2–3 times that of Pt/C and were reported in several patents in terms of mass activity at 0.90 V under oxygen, as well at the more practical PAFC design points of 215 mA/cm^2 under atmospheric pressure air and 205 °C [55]. PAFC power plants today use ternary Pt-alloys supported on graphitized carbon as cathode catalysts. (It should be noted that much of the literature dealing with electrocatalysis in phosphoric acid electrolytes report activity values that are much lower than those obtained today in PEMFCs mainly because of the significantly reduced anion adsorption in PEMFCs.)

It was found in PAFC durability evaluations that the base element of the Pt-alloy gradually leached out over thousands of hours of normal fuel cell operation. The initial Pt-alloys were prepared using carbothermal reduction that resulted in a solid solution and in which rapid quenching of the smaller crystallites impeded them from forming true equilibrium structures. To rectify the problem, new catalysts were prepared by subjecting them to a slow annealing to produce ordered structures that were found to be stable for ∼9000 h at 205 °C [56]. This was in spite of their predicted instability based on thermodynamics. From the several ternaries that were evaluated for PAFC, ordered Pt-alloys of PtRhFe/C showed the highest enhanced activity and chemical stability over time [57].

Other commercial catalyst companies such as TKK (PtNiCo), NEChemCat (PtCu, PtFeCu, and PtFeCoCu), and Johnson Matthey (JM) (high loading catalysts) also worked on Pt-alloys and patented a number of binaries, ternaries, and quaternaries that claimed better catalytic activity and improved stability over Pt/C [14]. Some of the Pt-alloy catalysts exhibited voltage gains of the order of 25–40 mV in the kinetic regime (where the Tafel-slope was of the order of $RT/\alpha F$ = 90 mV/decade, with a reaction order of 1, and measured at operating temperatures of 180–205 °C). These results are very encouraging and provide us with a rational basis for expecting similar gains in ORR activity when applied to PEMFCs.

4.1.2. Fundamental studies on alloy catalysts in liquid electrolyte half cells

Most of the research into developing catalyst for PAFC was conducted on half cells (prepared as PTFE-bonded gas diffusion electrodes) or subscale fuel cells. Several research

groups evaluated the effect of acid electrolyte type on the ORR kinetics using catalyst-coated diffusion media. In a recent review, Johnson Matthey reported that the activity of Pt is independent of the electrolyte used including 1 M sulfuric acid, 0.1 M sulfuric acid and 0.1 M perchloric acid, [14] contrary to other reports in the literature [25,41]. It should be noted that the specific activities reported in these liquid electrolytes studies are lower (by a factor of 10) than that observed in PEMFC and RDE data shown in Table 4. Nevertheless, in terms of relative magnitudes, the Pt-alloys/C showed about three times the mass activity of Pt/C in all the acids.

In addition, rotating disk electrodes (RDEs) have been used in the past as a platform to conduct electrocatalyst studies on well-defined, smooth and single crystal or polycrystalline electrodes to obtain fundamental understanding and insights into factors such as structural sensitivity [41,49], surface composition of alloys [58], etc. Markovic et al. [11] reviewed ORR activities on single-crystal Pt and Pt-alloys and proposed that the enhancement of kinetics on the alloys was due to inhibition of hydroxide formation on Pt in the presence of an environment of oxide covered Ni or Co atoms above 0.80 V. Most recently, Stamenkovic et al. [58] have studied different surface compositions of the Pt_3Co and Pt_3Ni alloy in perchloric acid and sulfuric acid: one sample of Pt_3Co was sputtered and composed of 75% Pt on the surface and the other annealed and composed of 100% Pt or a ''Pt skin structure'' or surface skeleton caused by the exchange of Co atoms with Pt in the first few surface layers (demonstrated by low-energy ion scattering). They found that the Pt skin-surface showed similar features in cyclic voltammetry to Pt surfaces yet exhibited 3–4 times higher specific activity in perchloric acid. Stamenkovic et al. proposed that the enhanced activity was the electronic modification of Pt atoms atop the Co-rich layer. They also reported that the catalyst activity was a function of the anion adsorption of the electrolyte used. In addition, they found no evidence (for all the alloys) of a reaction mechanism, reaction order, or activation energy that was any different from that observed for polycrystalline Pt. These results are important in that the amount of Pt used in the catalyst could be reduced significantly if the core of the alloy particle was replaced with an inexpensive element. Corrosion of the base-metal core through the thin surface layer, however, is an obvious problem for the catalyst.

It was not considered easy to apply bulk alloy understanding directly to high-surface-area catalysts that are commonly used in practical fuel cells until the advent more recently of TF-RDEs with high-surface-area catalysts applied to them as thin films. TF-RDE studies have since been used to obtain specific and mass activity values for Pt and Pt-alloy catalysts and shown to produce results comparable to fuel cells when the data are evaluated judiciously (see Section 3.2.2).

Toda et al. [16] have conducted studies on thin layers of sputter-deposited PtNi, PtFe, and PtCo and reported extremely high-activity enhancement factors of 10–20, but their baseline Pt activity is a factor of 10 lower than what otherwise is reported in the literature, casting significant doubt on the validity of their measurements. Paulus et al. [12] have conducted kinetic studies on high-surface-area Pt-alloy catalysts such as Pt/Vulcan, PtNi/Vulcan, Pt_3Ni/Vulcan, PtCo/Vulcan, Pt_3Co/Vulcan, and $PtRh_{0.3}Fe_{0.7}$/C and compared the activity gains for the ORR to that obtained on bulk Pt and Pt-alloys. Specific activity (i_s) enhancements of a factor of 2–4 compared to Pt were found in these studies. It was also found in these works that the rate-determining step in the ORR as well as apparent activation energies appears to be the same for the Pt-alloys as that on Pt.

It should be noted that there are many differences in conducting tests using a liquid electrolyte like phosphoric acid, sulfuric acid, or perchloric acid to simulate the environment of MEAs in PEMFCs. While it was shown in Section 3 that ORR activities similar to those in PEMFCs can be obtained for TF-RDE measurements in non-adsorbing $HClO_4$ electrolyte, there are significant experimental difficulties with respect to contamination in RDE set-ups, and the use of high scan rates in RDEs as opposed to obtaining steady-state data over 15-min periods in PEMFCs is problematic. TFMSA as an electrolyte would be a closer simulation of a Nafion membrane and although some work has been conducted with it there are issues of purity that plague it [59–61]. As a result, absolute activity values, with any degree of confidence, can be gained primarily from in situ fuel cell tests with the caveat that a high-quality catalyst layer must be prepared with a high utilization of the catalyst as described in the previous section.

4.1.3. Alloy catalysts in proton exchange membrane fuel cells (PEMFCs)

In the early 1990s, Texas A&M [30,52] investigated several binary Pt alloy systems such as PtNi, PtCo, and PtCr in small-scale fuel cells to characterize kinetic parameters complemented by several X-ray techniques to examine lattice parameters, stability, and the nature of surface species. The catalysts were alloyed at 900 °C, were composed of 20 wt.% Pt on Vulcan carbon, and, were manufactured into electrodes having 0.30 mg_{Pt}/cm^2 loadings. Testing was carried out under H_2–O_2 in the pressure range 100–500 kPa_{abs} and temperature range 40–80 °C. Table 2 in their paper reports results at 500 kPa of O_2 at 95 °C and for cathode catalyst loading of 0.30 mg_{Pt}/cm^2. The results indicated that 20–30 mV activity gains over Pt/C could be obtained due to a 2.4–3.6-fold increase in specific activity and a 2–3-fold increase in mass activity of the Pt-alloys, with PtCr/C having the highest activity. We note that the electrochemical surface areas of the electrodes in these studies were quite low (roughness factor of 61 cm^2_{Pt}/cm^2 for loadings of 0.30 mg_{Pt}/cm^2 which corresponds to ~20 m^2/g_{Pt} for Pt with values as low as ~12 m^2/g for PtCo/C). The specific activity at 0.90 V and 500 kPa_{abs} of total oxidant pressure (p_{O_2} = 420 kPa at 95 °C assuming 100% RH) was

calculated to be 360 μA/cm^2 for Pt/C. Today's state-of-the-art MEAs prepared using commercial Pt/C have specific activities of 180–210 μA/cm^2 at 0.90 V, p_{O_2} = 100 kPa and 80 °C. There are several corrections that need to be applied to the correct for hydrogen partial pressure, oxygen partial pressure as well as the temperature in order to compare the two specific activity numbers. Nevertheless, taking into account simply the dominant effect of oxygen partial pressure, we would expect the data in this literature reference to be a factor of ∼4 higher at 420 kPa as compared to 100 kPa (assuming a reaction order of 1), whereas the factor is found to be only 2. (The correction for the hydrogen partial pressure from 420 to 100 kPa$_{abs}$ would require obtaining the activity at 0.923 V instead of 0.900 V thus lowering the activity even further.) We raise this issue mainly to demonstrate that not only it is difficult to obtain a normalized activity, but also the baseline activity for Pt/C reported in the literature is frequently low (see also Table 3). Furthermore, a calculation of mass activities from their data shows Pt/C to have an order of magnitude lower activity as compared to typical values reported more recently. Activation energies for Pt and Pt-alloys were found to be comparable and the reaction order values inconclusive. X-ray diffraction patterns of the Pt-alloy samples in their study showed that the Pt-alloys were predominantly ordered cubic Pt_3M phases. XPS spectra indicated the existence of Co on the surface as oxides and Cr as Cr_2O_3. Durability evaluations were carried out at 50 °C at 200 mA/cm^2 for periods of 400–1200 h with degradation rates of 20–30 μV/h.

Mukerjee et al. [62] have also reported another extensive set of values for five Pt-alloys (PtCr, PtMn, PtFe, PtCo, and PtNi – all 75:25 Pt:M stoics) in a subsequent paper. In this paper, the roughness factors at equal loadings of all the Pt and Pt-alloys (0.3 mg$_{Pt}$/cm^2) were improved to about 130–150 cm$^2_{Pt}$/cm^2 as were the activities for the Pt-alloys. The results indicated that 20–30 mV activity gains over Pt/C could be obtained or a 1.2–5.0-fold increase in specific activity and similar increase in mass activity of the Pt-alloys over Pt with PtCr having the highest activity. As before, applying partial corrections for the oxygen pressure to normalize the data to 100 kPa of O_2, we still find the specific activity of their Pt/C and alloys to be quite low.

Considerable work has also been carried out by Johnson Matthey between 1995 and 1997 [14,28] on binary alloys such as PtFe, PtMn, PtNi, PtCr, and PtTi alloys heat-treated to various temperatures and containing 20 wt.% Pt-alloy/Vulcan support with Pt:M ratio of 50:50. The formation of alloys was confirmed by lattice contraction or expansion of the FCC Pt lattice parameter at an atomic ratio of 50:50. The kinetic performance of these alloys and Pt was studied in MEAs tested in small cells (active area = 25 cm^2) under H_2–O_2 at 75 °C at 308/377 kPa$_{abs}$. About 25 mV activity gains were observed in the comparison of PtTi, PtMn, PtFe to Pt/C baseline which are comparable to that obtained previously in PAFCs. Catalysts with enhanced oxygen activity were also measured under H_2-air at practical fuel cell current densities and the 25 mV gain was again confirmed. The specific activities reported at 900 mV 308 kPa$_{abs}$ H_2 and 377 kPa$_{abs}$ O_2 varied from 50 to 300 μA/cm$^2_{Pt}$ with an enhancement of a factor of ∼4 for the best (PtTi, PMn, and PtFe; specific activities in the range 330-400 μA/cm^2) Pt-alloys over platinum. We note again that the baseline Pt/C was reported to have an average specific activity, i_s, of ∼127 μA/cm^2 which (i_s, when normalized to p_{O_2} = 100 kPa$_{abs}$ is only ∼37 μA/cm^2) is about a fifth and mass activity about a tenth (i_m, when normalized to p_{O_2} = 100 kPa$_{abs}$ is only ∼0.010 A/mg$_{Pt}$) of that obtainable today in a state-of-the-art MEA. (Again, correction for the hydrogen partial pressure from 340 to 100 kPa$_{abs}$ would require extrapolating the activity at 0.918 V instead of 0.900 V thus lowering the activity even further.) The Pt and Pt-alloys in the study exhibited fairly linear Tafel-plots with slopes of ∼60 mV/dec.

Electron probe microanalysis (EPMA) was employed to evaluate the stability of the alloys. The Cr and Ti alloys did not show any apparent leaching from the catalyst to the membrane or anode catalyst layer while the PtFe, PtMn, and PtNi all showed leaching of the base-metal into the MEA, but no performance loss was observed over the 200 h of testing. Based on these results they tested the PtCr formulation using a higher 40 wt.% Pt/Vulcan and a composition of Pt:Cr of 75:25 for ease of alloying. These catalysts were tested in large area stacks of ∼240 cm^2 at 306 kPa$_{abs}$ absolute pressure and temperature of 80 °C. The O_2 curves showed the expected benefit of 20–30 mV at all current densities but the air curves did not show a corresponding increase for the Pt-alloy. They subsequently used a hydrophobic additive to obtain the same gains under air as under oxygen and demonstrated operation for 500 h. These results are typical in that Pt-alloy catalysts/C have a tendency to flood more easily than Pt/C under air and at high current densities. This phenomenon was attributed to the hydrophilic nature of the hydrous oxides formed on the base-metal surface of the Pt-alloy catalyst particles.

From this brief survey of literature data for PAFC, bulk and high-surface-area half cell studies in acids, and PEMFCs it appears that Pt-alloy catalysts can enhance the ORR specific activity (μA/cm$^2_{Pt}$) by a factor of 2–4. A corresponding increase in mass activity (A/mg) is achievable if the electrochemical surface area is maintained at the same levels as for Pt/C (70–90 m^2/g). Thus, the use of Pt-alloy catalysts to enhance activity and lower costs is a feasible approach for implementation in practical PEM fuel cell stacks.

4.2. Concerns specific to the use of alloy catalysts in PEMFCs

4.2.1. General concerns specific to the use of alloy catalysts in PEMFCs

In this section, we address fundamental and practical concerns and issues specific to applying Pt-alloy catalysts to PEMFCs. PEMFCs, in general, differ from PAFCs and other

liquid electrolyte fuel cells in several ways: (i) they operate at lower temperatures of 65–95 °C, (ii) anion adsorption on the catalyst is significantly lower than in phosphoric acid or sulfuric acid, (iii) they have a thin ionomer membrane (~25 μm) that separates the anode from the cathode. The membrane (density = 2 g/cm^3, 1000 EW) has about 5 μmol/cm^2 of H^+ sites. This value is about a tenth of the number of sites in a typical PAFC, severely limiting the number of ion-exchange sites that are available and thereby rendering it sensitive to contamination. (iv) The electrodes or catalyst layers (anode and cathode) are also fairly thin (~10–15 μm) and are composed of about 20–30 wt.% of similar ionomer to that in the membrane. The number of protonic sites in the catalyst layer (~0.5 μmol/cm^2) is now a tenth of that in the membrane, making it even more susceptible to contamination by cations.

The limited amount of ion-exchange sites especially in the catalyst layer (~0.5 μmol/cm^2) makes the MEA highly susceptible to poisoning by cations that may be introduced from any source such as the corrosion of bipolar plates or leaching of non-noble base elements incorporated in Pt-alloy catalysts [63,64]. If a large proportion of protonic sites are displaced by foreign cations, the protonic conductivity of the catalyst layer will be degraded, leading to higher ohmic losses and also to a lowering of the activity of Pt in the contaminated ionomer. For example, an electrode with 0.20 mg$_{Pt}$/cm^2 of a PtX-alloy has 1 μmol/cm^2 X that can replace 2 μmol H^+/cm^2 (assuming, e.g. Co^{2+}); this amounts to four times the number of H^+ sites available in the catalyst layer with the obvious risk of completely ion-exchanging and contaminating the catalyst layer. Thus one has to be very careful in modifying a Pt catalyst with base-metals that might leach out and contaminate the MEA in PEMFCs. It should be noted that Pt-alloys such as PtRhFe/C have been known to leach out over time in PAFCs, but have not resulted in a performance loss due to the large electrolyte inventory in these cells [57].

4.2.2. Leaching of non-noble elements in Pt-alloys

As we mentioned, cations introduced in a PEMFC readily ion-exchange with the protonic sites in the ionomer of the catalyst layer and membrane. The possible ramifications of this exchange of protonic sites with the base-metal cation that is leached out of the Pt-alloy catalysts are (i) a lowering of conductivity of the membrane due to dehydration leading to higher membrane resistance, (ii) an increase in the resistance of the cathode catalyst layer due to higher ionomer resistance, (iii) a lower diffusion of oxygen in the ionomer in the catalyst layer, and (iv) degradation of the membrane in the presence of certain metal cations such as Fe and Ti. A combination of the above factors, that may be hard to separate, will essentially lower the overall performance and accelerate the degradation of the fuel cell. Therefore, Mukerjee et al. [15] have proposed pre-leaching of the alloy to minimize the contamination of the MEA during operation.

There are at least three possible causes for the leaching of base-metal from a Pt-alloy/C catalyst in PEMFCs: (i) excess base-metal deposited onto the carbon support during preparation, (ii) incomplete alloying of the base element to Pt due to a low alloying temperature applied during formation of the alloy, (iii) even a well-alloyed base-metal may leach out of the surface under PEMFC operating conditions and leave a Pt-enriched surface or skin since thermodynamically base-metals are unstable under PEMFC potentials in acidic electrolytes (even Pt-alloys do not have high enough heats of mixing to confer stability).

A simple ex situ test was devised to estimate the leaching tendencies of several Pt-alloy catalysts. A measured sample of the alloy catalyst was immersed in 0.5 M H_2SO_4 at 90 °C under air for a period of 24 h. (In separate experiments, some of the Pt-alloy catalysts were leached for longer periods of time and it was found that 24 h was sufficient to leach out the base-metal with no further dissolution at longer periods of time.) The electrolyte roughly mimics the acidity of the ionomer in the catalyst layer and the presence of oxygen imposes a potential on the Pt-alloy catalyst mimicking electrochemical conditions expected under fuel cell operation. Fig. 10 shows the results of leaching experiments carried out on some experimental TKK Pt–Co/C catalysts. The unleached original Pt_xCo_{1-x}/C catalyst exhibited the greatest dissolution of the cobalt as measured from ICP analysis of close to 37% whereas the multiply pre-leached catalyst (preleached by TKK using a proprietary process suitable for larger batches) showed minimal leaching of less than 4%. A 4% leaching of the base element corresponds to an exchange of ~16% of the H^+ sites in the electrode and is within acceptable limits whereas 37% leaching would be sufficient to exchange with all the sites in the catalyst layer and then some. Needless to say, these estimates err on the side of caution since a portion of the leached cations

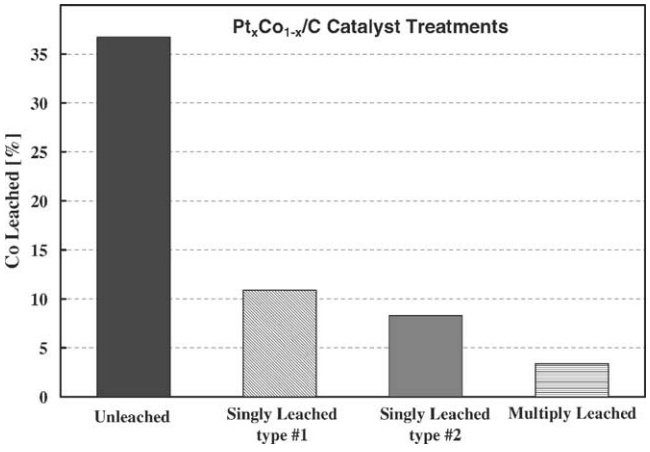

Fig. 10. Results of ex situ Pt-alloy catalyst leaching experiments carried out in 0.5 M H_2SO_4 at 90 °C under air for 24 h. The unleached Pt_xCo_{1-x}/C catalyst exhibits the greatest dissolution (~37% or 27 μmol g_{Pt}^{-1} h^{-1}) of the cobalt while the multiply pre-leached catalyst showed the least leaching (~4% or 2 μmol g_{Pt}^{-1} h^{-1}) as measured from ICP analysis of the leachate.

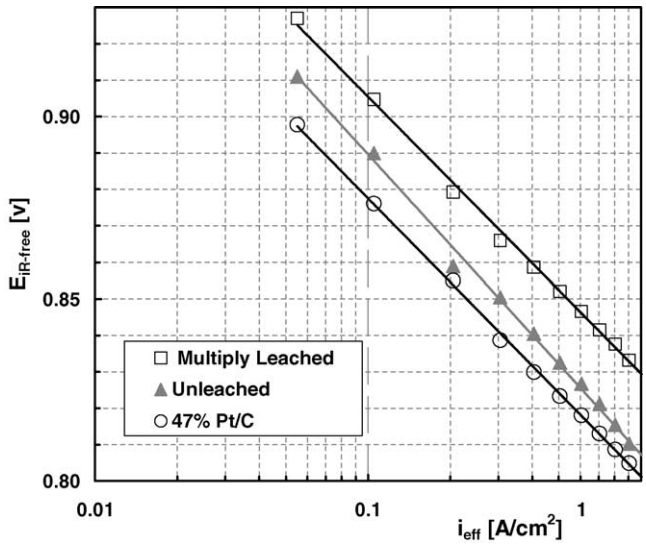

Fig. 11. *iR*-free (where R = resistance due to membrane, electronic components and contact resistance) *V–I* curves measured under H_2–O_2 (high stoics or low utilization) at total reactant pressures of 150 kPa_{abs} that were 100% humidified at 80 °C ($p_{O_2} \sim 100\ kPa_{abs}$) in 50 cm^2 active area cell hardware. The multiply leached Pt_xCo_{1-x}/C shows the highest catalytic activity over the entire range of current densities as compared to Pt/C under similar operating conditions. All MEAs catalyst loadings of 0.4/0.4 mg_{Pt}/cm^2 nominal loading.

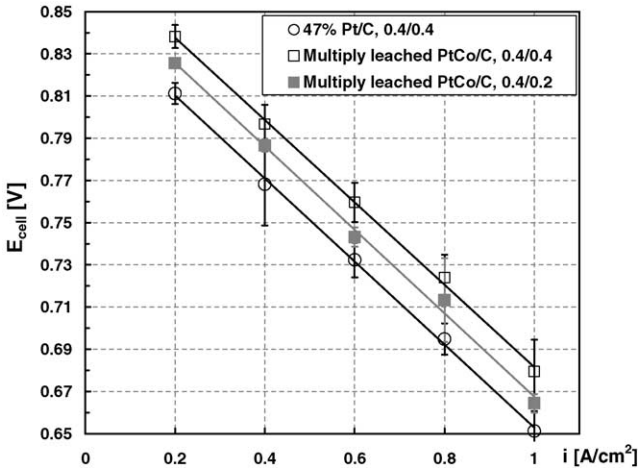

Fig. 12. Average beginning of life (BOL) stack cell performance of various Pt/C and Pt_xCo_{1-x}/C MEAs tested in a short stack (active area = 465 cm^2) under H_2-air at a cell temperature of 80 °C, and total reactant pressures of 270 kPa_{abs} with anode and cathode humidities at 100 and 50% and anode and cathode reactant stoichiometries of $s = 2/2$. The stack consisted of three type of cathodes on the MEAs (i) 0.40 mg/cm^2 Pt/C; (ii) 0.40 mg/cm^2 Pt_xCo_{1-x}/C – multiply leached; (iii) 0.20 mg/cm^2 Pt_xCo_{1-x}/C – multiply leached; all anodes had loadings of 0.40 mg/cm^2 Pt and the membrane thickness was 50 μm. Data shown are averaged over four cells of each type of MEA.

would diffuse and contaminate the protonic sites in the membrane itself. Based on the results of these leaching tests, the original and multiply leached Pt_xCo_{1-x}/C catalysts were selected for further assessment in sub-scale 50 cm^2 active area cell hardware for an evaluation of catalytic activity under oxygen. It should be noted here that other acid compositions might be required for Pt-alloys with more stable base-metal oxides (e.g., alloys containing Ti, Cr, etc.).

4.3. 50 cm^2 MEA cell testing

Some of the more promising leached and unleached catalysts were tested in small 50 cm^2 single cells under oxygen to evaluate catalyst activity. The MEA preparation technique and testing protocol are outlined in Section 2. Fig. 11 shows *iR*-corrected *V–I* curves measured under these operating conditions. The polarization curve is linear for the Pt/C as well as the multiply leached Pt_xCo_{1-x}/C with a Tafel-slope of about ~70 mV/dec over the entire range of current densities measured. The multiply leached Pt_xCo_{1-x}/C shows the highest activity (with a gain of about 25 mV over Pt/C) over the entire range of current densities as compared to Pt/C under identical conditions. The cathode catalyst loading was 0.40 mg/cm^2_{Pt} and the electrochemical area of the Pt/C was about 70 m^2/g while that of the Pt_xCo_{1-x}/C was about 40–45 m^2/g. This corresponds to a specific activity of 550 μA/cm^2 (a factor of 3 w.r.t. 47% Pt/C, Table 2) and mass activity of 0.28 (a factor of 2.5 w.r.t. 47% Pt/C, Table 2) for the unleached–multiply leached Pt_xCo_{1-x}/C. The unleached MEA exhibits a slight drop in Tafel-slope at higher current densities possibly due to base-metal contamination of the catalyst layer. Based on the results of these small cells, a short stack was built with the multiply leached PtCo/C and Pt/C MEAs and tested for both cell performance and durability and electrochemical area diagnostics. Table 5 summarizes the electrochemical surface areas, specific activity, and mass activity for the baseline 47% Pt/C as well as Pt_xCo_{1-x}/C and the target activities required to meet automotive cost goals.

4.4. Short-stack testing

4.4.1. Performance of Pt_xCo_{1-x}/C alloy catalysts

Based on the positive results obtained on Pt_xCo_{1-x}/C in small cells, a large area (465 cm^2) short stack was built containing MEAs prepared using cathodes with PtCo/C alloys as well as a benchmark Pt/C catalyst (the 47% Pt/C catalyst listed in Table 2): (i) 0.40 mg/cm^2 Pt/C; (ii) 0.40 mg/cm^2 Pt_xCo_{1-x}/C – multiply leached; (iii) 0.20 mg/cm^2 Pt_xCo_{1-x}/C – multiply leached; all the anodes had 0.40 mg/cm^2 Pt/C and the membrane was 50 μm in thickness. The third set of MEAs with 0.20 mg/cm^2 were included since our final goal is to utilize a lower loading of Pt catalyst in the cathode without any loss in performance. Fig. 12 depicts the average cell voltage (over four cells each) versus current density for each of the three types of MEAs. The 0.40 mg/cm^2 Pt_xCo_{1-x}/C multiply leached MEAs showed an improved performance of 25 mV versus the 47% Pt/C baseline MEAs over the entire current density range. In the range of catalyst loadings 0.05–0.50 mg/cm^2, a 20 mV change in voltage is theoretically expected for a change in loading by a factor of 2. Thus, owing to the ca.

Table 5
Summary of average catalyst loadings, electrochemical surface areas, specific activities, and mass activities

Catalysts	47% Pt/C (TKK)	46% Pt/C (TKK)	Pt_xCo_{1-x}/C (TKK)	Target Pt-alloy/C
Anode/cathode (mg_{Pt}/cm^2)	0.4/0.4	0.4/0.4	0.4/0.4	0.05/0.10
$A_{Pt,MEA(ca)}$ (m^2/g_{Pt})	70	80	50	70
rf (cm^2_{Pt}/cm^2)	280	320	200	70
$i_{s(0.9\ V)}$ ($\mu A/cm^2_{Pt}$)	180	210	550	720
$i_{m(0.9\ V)}$ (A/mg_{Pt})	0.11	0.16	0.28	0.44

Specific activities, $i_{s(0.9\ V)}$, and mass activities, $i_{m(0.9\ V)}$ were determined at 0.9 V and 80 °C at an O_2 partial pressure of 100 kPa_{abs} for 47% Pt/C baseline reported in this study, state-of-the-art 46% Pt/C baseline, Pt_xCo_{1-x} and target to be met.

two-fold higher mass activity of the Pt_xCo_{1-x}/C catalyst, the 0.20 mg/cm^2 Pt-alloy cathode MEAs would be expected to perform about as well as the 47% Pt/C baseline cathodes with loading of 0.40 mg/cm^2. In actuality, their performance fell slightly above that of the baseline 47% Pt/C. The operating conditions for the stack was H_2-air at 80 °C, 270 kPa_{abs} with anode and cathode humidities at 100 and 50%, respectively, and stoichiometries of $s = 1.3/2$. Since only H_2-air data were obtained on the short stack, a certain amount of mass-transfer loss is superimposed on the data even at low current densities. Fig. 12 depicts the average cell voltage (over four cells each) versus current density for each of the three types of MEAs. Fig. 13 is a plot of typical cyclic voltammograms taken in situ on individual cell cathodes, of the short stack, to measure the hydrogen adsorption or electrochemical area. The Pt_xCo_{1-x}/C typically exhibit lower areas than Pt/C because the initial particle size of the Pt-alloys are higher than that for Pt/C, as they generally undergo a heat treatment in their preparation. We note also that the Pt-alloys have hydrogen adsorption peaks that are smeared as compared to Pt/C. These electrochemical area measurements were made several times over the life of the stack under durability testing.

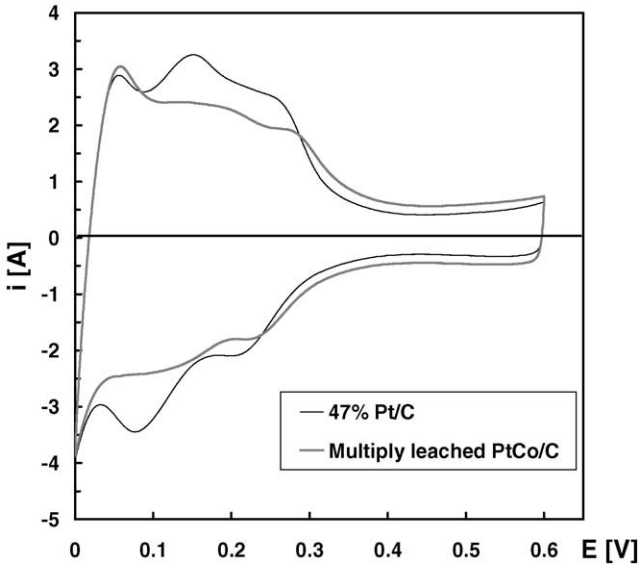

Fig. 13. Typical in situ electrochemical surface area measurement (m^2/g_{Pt}) for Pt/C and Pt_xCo_{1-x}/C. Measurements were carried out in a fuel cell short stacks with humidified 16% H_2 on the reference/counter side and humidified N_2 on the working electrode (cathode) at 25 °C and a voltage scan rate of 20 mV/s. The hydrogen adsorption area taken in the reducing sweep was measured between ~0.40 V and the plateau just prior to hydrogen evolution reaction starts (~0.05 V).

4.4.2. Durability of Pt_xCo_{1-x}/C alloy catalysts

Fig. 14 shows the durability of the baseline Pt/C and multiply leached Pt_xCo_{1-x}/C MEAs tested in a short stack (465 cm^2) under H_2-air at 80 °C, 270 kPa with anode and cathode humidities at 100% and stoichiometries of $s = 2/2$ (average voltages for four MEAs of each type; standard deviations are indicated by the error bars). The degradation rate is reported at 0.20 A/cm^2 over a period of 1060 h. First, we observe that the enhancement or performance offset of ~15–25 mV between the Pt/C and the Pt_xCo_{1-x}/C is maintained throughout the ~1000 h of stack operation within limits of error. We also observe that the degradation rate of the Pt/C and Pt-alloy/C MEAs are comparable at about 50 and 60 μV/h. Not shown is the membrane resistance of the MEAs which stayed essentially constant throughout the duration of testing indicating no degradation of the membrane due to contamination.

Fig. 15 shows the surface areas of Pt/C and multiply leached Pt_xCo_{1-x}/C MEAs tested in the short stack at the

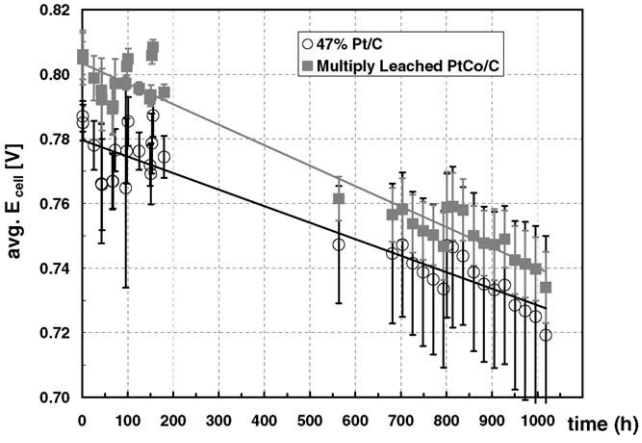

Fig. 14. Durability of Pt/C and Pt_xCo_{1-x}/C MEAs tested in a short stack (active area = 465 cm^2) under H_2-air at a cell temperature of 80 °C, and total reactant pressures of 150 kPa_{abs} with anode and cathode humidities at 100% anode and cathode reactant stoichiometries of $s = 2/2$. Data are shown with stack under a constant current density load of 0.20 A/cm^2 over ~1000 h. Data are averaged over four cells of each type of MEA.

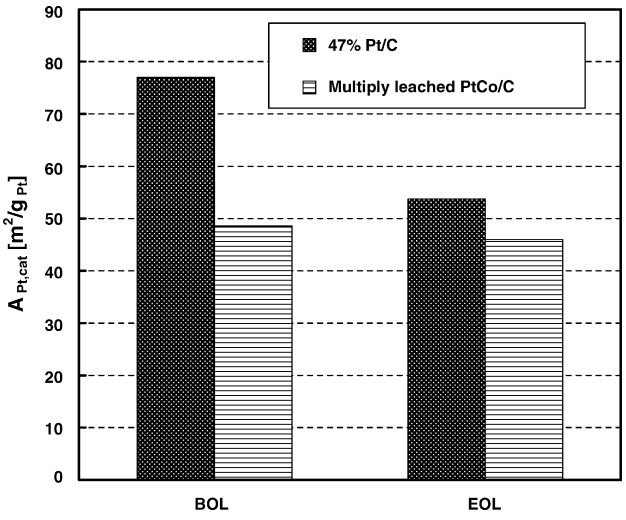

Fig. 15. In situ electrochemical surface area measurement (m^2/g_{Pt}) for Pt/C and Pt_xCo_{1-x}/C was carried out in a fuel cell short stacks with humidified 16% H_2 on the reference/counter side and humidified N_2 on the working electrode (cathode) at 25 °C and a voltage scan rate of 20 mV/s. Surface areas of Pt/C and Pt_xCo_{1-x}/C at the beginning of life (BOL) and at 1060 h (EOL) are shown for the Pt/C and Pt_xCo_{1-x}/C types of cathodes.

beginning of life (BOL) and at the end of ~1000 h (EOL) of operation. Data is averaged over four cells of each type of MEA in the stack and shows that the surface area loss for the Pt_xCo_{1-x}/C catalyst is lower than that for Pt/C measured over the ~1000 h of operation. These results indicate that the Pt-alloy catalyst starts life with a larger particle size and does not sinter as rapidly as the Pt/C. This preliminary result is encouraging in terms of durability of the Pt-alloy.

This measured loss in electrochemical surface area can be converted into an equivalent loss in cell voltage using the Tafel equation (ΔE_{loss} = 70 mV log(area loss)). The calculated loss in cell voltage as a result of particle size growth or loss in electrochemical surface area is associated purely with kinetics and is found to be ~11 μV/h for Pt/C and ~2–3μV/h for Pt_xCo_{1-x}/C. Thus, out of the total degradation rate of about ~50 μV/h, a significant portion (>80%) of the losses is associated predominantly with factors related to mass transfer. In principle, these losses can be reduced or eliminated by optimizing the electrode structure, changing the operating conditions, and/or changing the hardware flow-field designs.

4.5. Conclusions/future work

Based on the positive results of alloy catalyst activity enhancement obtained in liquid electrolyte fuel cells (i.e., PAFCs), similar alloy catalysts have been studied in the more contamination-sensitive PEMFC stack environment with promising results. Catalyst activity results on Pt_xCo_{1-x}/C under H_2–O_2 measured in small cells as well as H_2-air in short stacks in this study is promising and show: (i) pre-leaching of Pt-alloy catalyst before MEA preparation removes base-metal deposited on the carbon surface or poorly alloyed to the Pt, (ii) ca. three-fold enhancement of specific activity is observed at this point in time, (iii) a ca. 2.5-fold enhancement of mass activity is observed compared to Pt catalyst supported on comparable carbons, (iv) durability over ~1000 h is comparable for the Pt-alloys and Pt/C, (v) contamination and deactivation of the catalyst is negligible due to catalyst leaching over the 1000 h testing, and (vi) catalyst sintering or particle size growth is slower in Pt_xCo_{1-x}/C alloys than in Pt/C.

Future work requires: (i) synthesizing Pt-alloy/C catalysts with improved electrochemical surface areas comparable to Pt/C (i.e., 70–90 m^2/g) to obtain the four-fold enhancement of mass activity over Pt/C; this may in part be achievable through the use of lower weight percent Pt-alloy/C (20–35 wt.%) in low-loaded (0.10–0.20 mg/cm^2) catalyst layers, (ii) improving mass transfer (lowering flooding) in the catalyst layer by optimization of the structure in terms of ionomer/C ratio. Using a lower weight percent Pt-alloy/C (20–35 wt.%) in low-loaded (0.1–0.2 mg/cm^2) catalyst layers would permit the use of catalyst layers of comparable thickness to 0.4 mg/cm^2 Pt/C, thus distributing the water generated in reaction over a greater volume for easier removal.

5. Platinum-free catalysts

5.1. Performance requirements for potential non-platinum electrocatalysts

We have seen that economic viability for automotive applications of fuel cells based on the very expensive metal Pt requires that one be able to reliably extract a very high and stable level of activity from each Pt atom over 5500 h of intermittent operation. Platinum alloys, which can at least initially increase the activity of each Pt atom to the required level, must still demonstrate the requisite long-term stability.

Common sense would seem to require that one also consider using, instead of a strictly minimized amount of an expensive catalyst such as Pt, a significantly larger amount of a much cheaper, if less active, catalyst. If this catalyst were sufficiently inexpensive, one could perhaps afford to use significantly more than the amount required for the initial kinetic activity. For such a heavily loaded system, one might expect that a modest but continuous rate of catalyst degradation would then have minimal impact on the fuel cell performance. The search for this particular Holy Grail of the cheap non-Pt cathode electrocatalyst has proceeded now through at least four decades, and a review to which one of the current authors contributed in 1982 [65] is still not hopelessly out of date. Since few electronically conductive non-noble materials are stable in the acidic (and fluoride-ion-containing) PEMFC environment [66], most work, and certainly most of the success, on non-noble oxygen reduction catalysts has been in alkaline electrolytes. For PEMFCs, the acid stability criterion alone rules out all particles of non-noble metals and most, if not all, oxides.

Some limited success in acid on both the stability and activity fronts has been achieved with a class of materials in which a transition metal ion, typically Fe or Co, is stabilized by several nitrogens bound into an aromatic or graphite-like carbon structure. The appropriate form of carbon has generally been derived from polymerization (and often pyrolysis) of organic macrocycles akin to the active center of hemoglobin. Examples of such ''macrocycle'' catalysts are polymerized iron phthalocyanine [67,68] and cobalt methoxytetraphenylporphyrin [69]. The activity of such materials has typically improved after heat treatments at temperatures sufficiently high to remove most of the hydrogen and much of the nitrogen from the macrocycle precursors, leading to significant controversy over the nature of the active site. Dodelet and coworkers [17–19] have prepared materials with interesting activity that lasted at least 24 h in a PEMFC by heating carbons in a gas mixture containing ammonia and treating this carbon with iron compounds. From results of secondary ion mass spectroscopy and other analytical techniques, they identified the most active site as Fe (in an oxidized state) coordinated to two pyridinic nitrogens at the edge of a graphene sheet [19]:

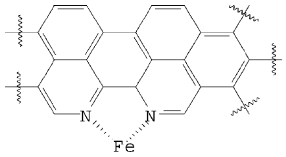

[6]

Proposed active site, after Ref. [17]. The remaining coordination of the Fe remains undetermined.

5.2. Minimum activity requirements

Can such materials have adequate activity for application in automotive fuel cells? We have discussed the critical automotive requirements for non-Pt catalysts elsewhere [70,71]; here we summarize. The comparison of activity of catalysts with disparate compositions and structures is fraught with difficulties. The most rigorous comparison between catalysts can be made if one can quantify two factors for each catalyst: (1) the turnover frequency (TOF), or electrons transferred per active site per second at a given potential and conditions, and (2) the volumetric site density (SD), in active sites per cm^3 of supported catalyst. For a catalyst layer thickness τ (cm), the current density i (A/cm^2) equals $(1.6 \times 10^{-19}) \times \text{TOF} \times \text{S.D.} \times \tau$, where the numeric factor is the charge on the electron in coulombs. The next paragraph will show that it can also be useful to think in terms of current per unit *volume* of supported catalyst (A/cm^3), which equals $(1.6 \times 10^{-19}) \times \text{TOF} \times \text{S.D.}$ It should be noted that novel catalysts have seldom been evaluated under the standard conditions discussed in the first section of this paper, and insufficient data are usually available to allow extrapolation of the behavior of the novel catalyst to different operating conditions. To make a comparison to Pt, one therefore uses the known temperature and pressure dependencies of Pt to correct the activity of the novel catalyst to standard conditions. This approach, while not rigorous, provides a first-order feel for how close or far the novel catalyst activity lies from practical utility and will have to suffice until data on the novel catalysts is available under the reference fuel cell conditions. Since non-Pt catalysts seldom, if ever, show measurable activity at 900 mV RHE (where mass-transport effects for Pt can be neglected), comparison will be made to Pt at a cell-resistance-corrected potential of 800 mV RHE (where mass-transport effects should still be small).

If a cathode catalyst were free, how much of it could one afford to use? This question, which is nowhere near as silly as it might at first appear to be, is central to the proper evaluation of non-Pt catalysts. Given the limited space available in an automobile, one cannot simply increase the stack area to accommodate a less active catalyst. A two-fold larger area than required under the path to $<0.2\ g_{Pt}/kW$ shown in Table 1 corresponds to about the maximum volume that one could expect to fit in a light-duty vehicle. And Pt is not the only costly material used in a PEMFC. Even at the cost levels projected for the mass production of millions of PEMFC vehicles per year, the cost of increased area (membrane, diffusion media, bipolar plate, etc.) would likely exceed the savings from avoiding Pt-based catalysts with activities corresponding to $<0.2\ g_{Pt}/kW$ at less than the two-fold area expansion just mentioned. One can also get more catalyst into a stack by increasing the electrode layer thickness, but here one faces a technical limit of perhaps at most 10 times the ~10 μm current state-of-the-art electrode layer thickness before mass-transport limitations would become debilitating. The maximum total volume that the costless catalyst could occupy is therefore $2 \times 10 = \sim 20$ times the volume of the reference 47% Pt/C cathode catalyst in Fig. 4 (grey circles), the activity of which, in turn, needed to be doubled (at minimum) for automotive viability. Considering all these factors, the activity of a costless cathode catalyst (per unit *volume* of supported catalyst, i.e., A/cm^3) for automotive applications needs to be no less than ~1/10th of the current industrial Pt activity exemplified by the data of Fig. 4 (grey circles) at equivalent conditions.

5.3. Reported activities of non-Pt catalysts

Some of the highest oxygen reduction activities documented for a non-Pt catalyst in a PEM fuel cell have been shown by Faubert et al. [17, Fig. 3], reproduced here as Fig. 16. These data, giving 0.038 A/cm^2 at 800 mV (versus RHE, corrected for cell resistance), were taken in a 1-cm^2 PEM fuel cell at 50 °C with fully humidified hydrogen and oxygen pressures of 310 and 510 kPa, respectively, on an ammonia-treated carbon catalyst layer containing 1.6×10^{17} atoms of iron. The carbon support was obtained by pyrolyzing perylenetetracarboxylic dianhydride (PTCDA).

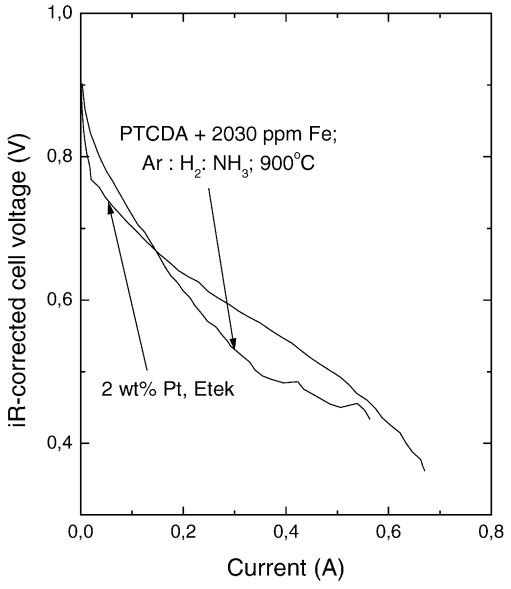

Fig. 16. Activity of 7.3 mg of an iron/ammonia-treated carbon (from PTCDA) catalyst in a 1-cm^2 PEM fuel cell (Nafion^{TM} 117) at 50 °C (humidifiers at 105 °C), operating pressures 310 kPa H_2, 510 kPa O_2. Also shown is performance measured for 7.3 mg of a commercial 2% Pt/C catalyst. Reproduced from Ref. [17].

Faubert et al.'s observations that activity increased with iron content up to 0.5% but then leveled off make reasonable an assumption that at the Fe concentration of Fig. 16 (2030 ppm) essentially all of the iron was active. With this assumption, a turnover frequency of 1.45 e^-/(Fe s) at the conditions of the measurement can be calculated (Table 6). Correcting to the reference conditions of 80 °C, 100 kPa p_{O_2} using Pt-based factors of p_{O_2} to the first order and E_a = 54.7 kJ/mol$_{O_2}$ [72] one calculates a corrected TOF for Fe/PTCDA of 1.7 e^-/(Fe s), i.e. ~1/15th of that for reference industrial Pt. It should be noted that this small net adjustment for conditions results from opposing corrections of 5.6× for temperature and 1/4.8× for oxygen partial pressure (water vapor pressure subtracted from cathode operating pressure), and that a large spread is found for literature values of the activation energy for oxygen reduction on Pt (at least 22 kJ/mol [12] to 76 kJ/mol [30]). These extremes of E_a's would lead to temperature correction factors for 50 °C → 80 °C ranging from 2× to 11×. This five-fold uncertainty becomes 40-fold when correcting data from 21 °C → 80 °C, as done below. Comparison between data taken at different temperatures is therefore clearly dangerous, and the comparisons here should be considered to be only order of magnitude estimates. This situation points out the urgency of taking data for innovative catalyst systems at the temperature range of interest for automotive fuel cells using current membrane technology, i.e., 60–80 °C.

For the Fe/PTCDA catalyst of Fig. 16, if one assumes the carbon layer density of 0.4 g/cm^3 seen for industrial MEAs (see below), then the site density can be calculated as 9 × 10^{18} Fe/cm^3. This is ~1/35th that of reference industrial Pt (Table 6) and was limited by the number of proper nitrogen sites in the ammonia-treated carbon support.

Fig. 16 indicates that in Faubert et al.'s experiments, the activity of the Fe catalyst exceeded that of a similarly tested commercial 2% Pt/C catalyst above 0.67 V RHE. If one assumes a reasonable 25% dispersion (60 m^2/g) for this reference Pt catalyst, Table 6 shows that its condition-corrected turnover frequency would be less than 1/25th of that for the reference industrial Pt catalyst discussed in the first section of the current paper (47% Pt/C catalyst in Table 2). Quantitative inspection of papers in the electrocatalyst literature shows that, in quite a few cases, reference Pt catalysts have given activities well below the true state-of-the-art intrinsic oxygen reduction capabilities of Pt. In all catalytic studies, it is important that reference catalysts be shown to perform to their full known capabilities before the performance of another catalyst is measured. "Better than measured for Pt" does not mean much if that Pt is badly poisoned or otherwise performs below its known capabilities. One really cannot make the assumption that catalysts of widely differing compositions would be equally affected by performance-crippling test conditions. In the discussion to follow, we will carry forward the absolute

Table 6
Turnover frequencies (TOF) for O_2 reduction (e^-/(site s)), site densities, and their product × 1.6 × 10^{-19} (=A/cm^3 of supported catalyst) at 800 mV$_{iR\text{-free}}$ for baseline 47% Pt (from the data set of Fig. 4, grey circles) compared to activity requirements for a costless catalyst and the experimental absolute activities of non-Pt (and Pt) catalysts from Refs. [17,19,21]

	T (°C)	p_{O_2} (kPa$_{abs}$)	TOF (e^-/site s) at reported conditions	TOF (e^-/site s) at conditions of Fig. 4	S.D./10^{20} (sites/cm^3)	A/cm^3 at conditions of Fig. 4
47% Pt/C reference (Fig. 4, grey circles)	80	100	25	25	3.2	1300
"Costless catalyst" targets	80	100	2.5	2.5	3.2 or compensating higher TOF	130
Fe/PTCDA (Faubert et al. [17])	50	498	1.45	1.7	0.09	2.4
Fe–phenanthroline (Bron et al. [20])	21	100	0.023	1.0	0.49	7.8
Fe/PTCDA (Jaouen et al. [19])	80	498	0.11	0.023	0.09	0.03
2% Pt/C (Faubert et al. [17])	50	498	0.78	0.92	0.06	0.88
10% Pt/C (Bron et al. [21])	21	100	0.23	10	0.34	55
5% Pt/C (Jaouen et al. [19])	80	498	4.5	0.94	0.15	2.3

TOFs are shown both at the conditions of measurement and corrected to the reference industrial conditions of Fig. 4 assuming p_{O_2} to the first order and E_a = 54.7 kJ/mol$_{O_2}$ [72], i.e., corrected using parameters for Pt.

activity of the Fe/PTCDA catalysts shown in Fig. 16, not the relative activity versus Pt in that figure. And we will see that our procedure produces similar turnover frequencies for a similar novel catalyst prepared and tested under completely different procedures.

Table 6 compares turnover frequencies (as-measured and corrected), site densities, and (corrected) A/(cm^3 supported catalyst)'s for the Fe/PTCDA (non-Pt) and Pt results of Fig. 16 to those of reference industrial Pt. The properties of the industrial reference were listed in the first catalyst column of Table 2; its activity was calculated from the A/cm^2 shown for it at $E_{iR\text{-free}}$ = 800 mV in the Tafel-plot of Fig. 4. Also shown are the minimum automotive values proposed here as needed for a costless catalyst, i.e., 1/10th of the volumetric activity of reference industrial Pt. It can be seen that the turnover frequency from this unusually good non-Pt result of Faubert et al. [17] lies within a factor of ~1.5 of the automotive costless-catalyst requirement, but that the site density is about 35-fold lower than what is needed.

How much of an improvement in number of active sites per cm^3 could one reasonably expect for such catalysts? Similar catalysts prepared with higher Fe loadings gave no higher activity, presumably because the additional iron was not properly coordinated with nitrogen to give the most active catalytic moiety (drawn out in formula (6) above as proposed by the Dodelet group). The smallest organic molecule containing the proposed coordination site for iron (albeit with 2/3 H atom per C atom to be removed by pyrolysis) is 1,10-phenanthroline, with an N/C ratio of 1/6:

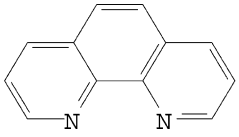

1,10-phenanthroline [7]

A typical carbon-black-based electrocatalyst with a carbon loading of 0.4 mg/cm^2 gives a catalyst layer thickness of about 10 μm, i.e., a carbon density of ~0.4 g/cm^3. *If* one could pyrolyze and polymerize 1,10-phenanthroline to give a high surface area, conductive material retaining *all* the nitrogen in the proper N_2 configuration, *if* one could coordinate an iron into each N_2 site (this would require 23 wt.% Fe), and *if* each of these sites had access to adequate paths for conduction of oxygen, electrons, and hydrogen ions, then one could theoretically achieve a maximum active site density of 1.3 × 10^{21} sites/cm^3. Coupled with a 1.7 e$^-$/(site s) turnover frequency, this site density could give 350 A/cm^3, almost three times the 130 A/cm^3 that would be needed for automotive use if one could maintain 100% utilization with a 100-μm electrocatalyst layer. So *if* the product of all of the "if's" listed above could be met simultaneously to give a net of at least 30% utilization of all of the nitrogen for a 100-μm electrocatalyst layer, then a non-Pt catalyst with the turnover frequency of Fe/PTCDA shown in Table 6 *just might* have enough activity to be used in automotive fuel cells.

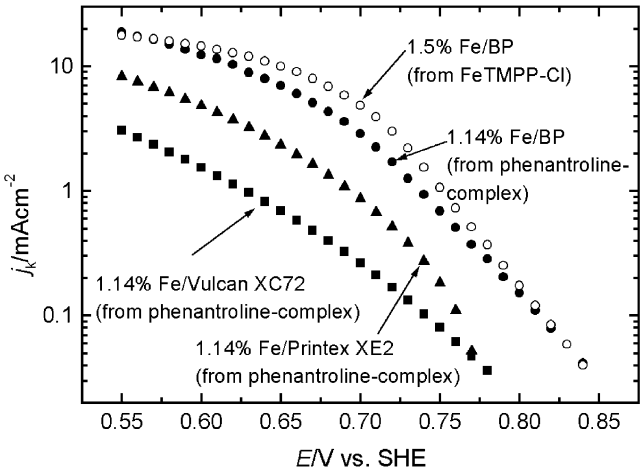

Fig. 17. Oxygen reduction Tafel-plot (log of kinetic current vs. potential) derived from Koutecky–Levich treatment of rotating disk data from 25 μg [73] of iron–phenanthroline-coated Black Pearls carbon black (1.14% Fe) (filled circles) on a 0.0707-cm^2 [20] glassy-carbon disk in oxygen-saturated 0.5 M H_2SO_4 at 21 °C. Reproduced from Ref. [21].

Bron et al. [20,21,73] have published rotating disk electrode results in 0.5 M H_2SO_4 at 21 °C, reproduced in Fig. 17, for carbon-black-supported catalysts derived from an iron 1,10-phenanthroline complex. The majority of their catalyst layer, however, consisted of a commercial carbon black rather than of pyrolyzed 1,10-phenanthroline, so the total nitrogen concentration could not have been as high as suggested in the preceding paragraph. At 800 mV versus RHE (since a highly conductive liquid electrolyte was used, it is not critical that no correction was made for cell resistance), Bron et al. showed a kinetic current of 0.16 mA/cm^2 [21] for a 0.0707 cm^2 electrode [20] containing 25 μg [73] of a 1.14% Fe catalyst, corresponding to a corrected turnover frequency of 1.0 e$^-$/(Fe s), similar to that derived from Faubert et al.'s data [17]. It should be noted that, because the Bron data must be corrected over a broader temperature range of 21 °C → 80 °C, the cautions previously raised about the uncertainty of the E_a for oxygen reduction make this correction even more uncertain than that applied to the Faubert et al. data. Despite using a commercial carbon black support, Bron et al. achieved a ~5-fold increase in site density versus Faubert et al. (again assuming a 0.4 g/cm^3 density for a catalyst layer based on carbon black). Nevertheless, the corrected A/cm^3 figure still falls about 20× short of the activity requirement for a costless automotive catalyst. If one could make a catalyst with less standard carbon black and more pyrolyzed phenanthroline that still maintained high dispersion of the active sites, one might push the initial A/cm^3 into the conceivably useful range. Bron et al.'s corrected turnover frequency for Pt (from data similar to Fig. 17) [21] giving i_k = 1.0 mA/cm^2 for 25 μg of 10% Pt) lies about 2.5-fold lower than that for the reference 47% Pt MEA catalyst, as one would expect for data taken in sulfuric acid. In the latter electrolyte the

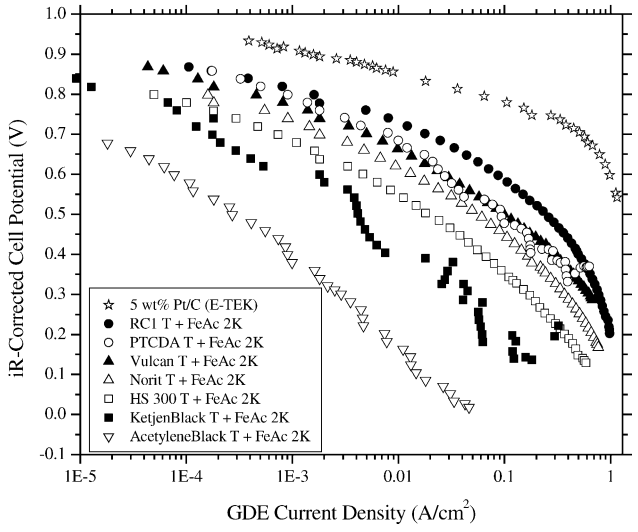

Fig. 18. Oxygen-reduction performance of a number of non-Pt catalysts (2.1 mg each), including Fe/PTCDA (open circles), in a 1-cm^2 PEM fuel cell at 80 °C (humidifiers at 105 °C), operating pressures 310 kPa H_2, 510 kPa O_2, compared to 5% Pt/C (stars). Reproduced from Ref. [19].

(bi)sulfate anions adsorb onto at least the (111) facets of Pt and reduce its oxygen reduction activity [25,53].

Fig. 18, once again from the Dodelet group [19], shows more recent fuel cell data for Pt and for the Fe/PTCDA catalyst under discussion (shown in the figure legend as "PTCDA T + FeAc 2K"), this time at 80 °C (requiring less extrapolation to standard conditions) and with 2.1 mg catalyst/cm^2. At 800 $mV_{iR\text{-corrected}}$ versus RHE, 2000 ppm Fe/PTCDA gave 8×10^{-4} A/cm^2 and 5% Pt gave 0.058 A/cm^2. The corrected Pt turnover frequency at 800 mV RHE is very close to that in Faubert et al. [17], but the corrected TOF for Fe/PTCDA is less than 1/50th of the earlier value. These more recent results lead to the more typical observation that non-Pt catalysts operate at significantly lower voltages for given current densities than even relatively low-wt.% Pt catalysts used at the same loading of total supported catalyst. If the currents at 800 mV drop below those presently achieved in state-of-the-art Pt fuel cells, then the efficiency at part load (where a vehicle spends most of its time) of a fuel cell automotive power plant would not be high enough to enable the fuel cell vehicle to have adequate overall fuel economy.

5.4. Non-Pt catalyst durability concerns and conclusions

It should be noted that, even if non-Pt oxygen reduction catalysts could fulfill the stringent requirements for absolute activity, they would still face durability challenges that surpass those confronting Pt-catalyst systems. All of the corrosion concerns previously raised for the non-noble components of Pt-alloy catalysts hold true for non-Pt catalysts as well. In addition, most non-Pt catalysts reduce a higher percentage of oxygen to hydrogen peroxide (rather than to water) than do Pt-based catalysts. Bron et al. [20,21] showed that their Fe-phenanthroline catalysts consumed less than $4e^-$ per O_2, particularly at lower electrode loadings. These results suggested a mechanism with a first $2e^-$ reduction step to peroxide followed (incompletely) by a $2e^-$ reduction step to water. Bron et al. ascribed the low durability of their catalyst (4.5-fold decrease in activity over 40 h) [20] to the attack of this peroxide on the catalyst itself.

The most active non-Pt oxygen reduction catalysts for acid electrolytes to date contain iron. Unfortunately, Fe^{2+} is an unusually effective catalyst for the conversion of hydrogen peroxide to the peroxyl radical [66]. The latter species is implicated in the primary mode of chemical degradation of the perfluorinated sulfonic acid membranes used in PEM fuel cells [66]. From the viewpoint of overall fuel cell durability, it therefore seems important to search for non-Pt catalysts completely free of leachable iron. Durability concerns seem, if anything, even more daunting to the feasibility of non-Pt PEM fuel cell cathode catalysts than are the already-tough activity issues.

The development of highly active and durable non-Pt oxygen reduction catalysts could remove one of the major cost factors that challenge the introduction of practical mass-market fuel cell light-duty vehicles. However, the first four sections of this paper have shown that the Pt cost issue need not stop the widespread automotive use of fuel cells if current data on Pt-alloy systems can be fully realized in durable systems. Other fuel cell cost considerations, plus volume constraints for automotive powertrains, require that even a costless catalyst have an activity no more than one order of magnitude lower than that of state-of-the-art Pt, expressed as A/cm^3 of supported catalyst. Results with non-Pt catalysts known to these authors to date have not shown the required activity, but a physically possible (if perhaps improbable) pathway to adequate activity through an increased density of active sites can be charted out. If the activity targets could be fully realized (including maintaining high utilization of catalyst layers up to 100 μm thick), then significant challenges with regards to durability would still need to be overcome. Continued fundamental, systematic work of the type reviewed here, combined with careful attention to the vehicular requirements for quantitation of *absolute* oxygen reduction catalyst activities at 60–80 °C and thoughtful testing of durability, are needed to determine whether the high-risk, but possibly high-reward, goal of non-Pt automotive fuel cell catalysts can eventually be realized.

6. Conclusions

Analysis of the voltage loss terms in state-of-the-art H_2/air MEAs shows that a significant increase in MEA performance could be realized by reducing the mass-transport-induced voltage losses at high current densities. It is shown that a 50% reduction of the currently observed mass-transport losses combined with a reduction of Pt-loadings to 0.05/0.1 mg_{Pt}/cm^2 (anode/cathode) would result

in MEA power densities of 0.7 W/cm^2 at <0.2 g_{Pt}/kW while maintaining high energy conversion efficiency at full power. Performance at these levels satisfies the automotive PEMFC development targets. However, in order to maintain a high energy conversion efficiency at medium- to low-power levels, improved cathode catalysts with an approximately four-fold higher activity compared to Pt/C are required. To guide cathode catalyst development, two different test methodologies for the quantitative determination of catalyst activity are proposed, and benchmark mass activities and specific activities for state-of-the-art Pt/C catalysts are presented. Analysis of Pt-particle size effects indicates that little or no mass activity gains are expected for catalysts with Pt surface areas exceeding the 90 m^2/g_{Pt} surface areas which are typical for state-of-the-art catalysts.

Catalyst activity results on Pt_xCo_{1-x}/C under H_2–O_2 measured in small cells as well as under H_2-air in short stacks in this study are promising and show that (i) pre-leaching of Pt-alloy catalyst before MEA preparation reduces the contamination during operation and has negligible effect over a lifetime of ~1000 h, (ii) ca. three-fold enhancement of specific activity and a 2.5-fold enhancement of mass activity is observed at this point in time for the Pt_xCo_{1-x}/C over Pt/C baseline, (iii) degradation rates over ~1000 h in a stack are comparable for the Pt-alloys and Pt/C, and (iv) catalyst sintering or particle size growth appears to be slower in Pt_xCo_{1-x}/C alloys than in Pt/C. At this point in time, the PEMFC development targets require a four-fold enhancement of mass activity and have not been achieved, but Pt-alloys/C catalysts appear to be a feasible pathway towards meeting them.

Non-Pt catalysts could contribute to an automotive solution if the product of their turnover frequency and volumetric active site density could be raised to within an order of magnitude of the baseline value for reference industrial Pt and if major durability issues could be solved. Initial turnover frequencies from two reports of iron-based catalysts appear to be within striking distance of the requirement, but site densities remain too low by a factor of 10–50. A physically plausible (if perhaps unlikely) pathway to adequate site density exists, but durability issues would probably require replacement of iron with another active center. Unless progress can be made on non-Pt catalysts more rapidly than past experience suggests, one must expect that the cathode catalysts for automotive fuel cells will contain some Pt.

Acknowledgements

We would like to thank John Doyle, Tom Faben, and Mike Scozzafava for their expert help in making all the MEAs tested in this study. Furthermore, we would like to thank Susan Yan for her invaluable contributions in the development of MEA preparation methods for low Pt-loadings. Much thanks goes to Jeanette O'Hara for her support in setting up the RDE test stand. Finally, thanks go to Tomoyuki Tada from TKK for providing the Pt-alloy catalyst samples.

References

[1] S.S. Kocha, Principles of MEA preparation, in: W. Vielstich, A. Lamm, H. Gasteiger (Eds.), Handbook of Fuel Cells – Fundamentals, Technology and Applications, vol. 3, Wiley, Chichester, UK, 2003, p. 538 (Chapter 43).
[2] D.J. Wheeler, J.S. Yi, R. Fredley, D. Yang, T. Patterson, L. VanDine, J. New Mater. Electrochem. Syst. 4 (2001) 233.
[3] D.A. Masten, A.D. Bosco, System design for vehicle applications: GM/Opel, in: W. Vielstich, A. Lamm, H. Gasteiger (Eds.), Handbook of Fuel Cells – Fundamentals, Technology and Applications, vol. 4, Wiley, Chichester, UK, 2003, p. 714 (Chapter 53).
[4] A. Rodrigues, M. Fronk, B. McCormick, Driving towards a successful future, in: W. Vielstich, A. Lamm, H. Gasteiger (Eds.), Handbook of Fuel Cells – Fundamentals, Technology and Applications, vol. 4, Wiley, Chichester, UK, 2003, p. 1172 (Chapter 85).
[5] M.F. Mathias, H.A. Gasteiger, Fundamental research and development challenges in polymer electrolyte fuel cells technology, in: Proceedings of the Proton Conducting Membrane Fuel Cells III Symposium, Salt Lake City, UT, Fall 2002, The Electrochemical Society, in press.
[6] C. Jaffray, G.A. Hards, Precious metal supply requirements, in: W. Vielstich, A. Lamm, H. Gasteiger (Eds.), Handbook of Fuel Cells – Fundamentals, Technology and Applications, vol. 3, Wiley, Chichester, UK, 2003, p. 509 (Chapter 41).
[7] J.S. Yi, J. Puhalski, C. King, Abstracts of the 202nd Meeting of the Electrochemical Society, vol. MA 2002-2, Abstract No. 812, The Electrochemical Society, Salt Lake City, UT, 2002.
[8] H.A. Gasteiger, J.E. Panels, S.G. Yan, J. Power Sources 126 (2004) 162.
[9] N.M. Markovic, The hydrogen electrode reaction and the electrooxidation of CO and H_2/CO mixtures on well-characterized Pt and Pt-bimetallic surfaces, in: W. Vielstich, H. Gasteiger, A. Lamm (Eds.), Handbook of Fuel Cells – Fundamentals, Technology and Applications, vol. 2, Wiley, Chichester, UK, 2003, p. 368 (Chapter 26).
[10] H.A. Gasteiger, W. Gu, R. Makharia, M.F. Mathias, B. Sompalli, Beginning-of-life MEA performance: efficiency loss contributions, in: W. Vielstich, A. Lamm, H.A. Gasteiger (Eds.), Handbook of Fuel Cells – Fundamentals, Technology and Applications, vol. 3, Wiley, Chichester, UK, 2003, p. 593 (Chapter 46).
[11] N.M. Markovic, T.J. Schmidt, V. Stamenkovic, P.N. Ross, Fuel Cells: Fundam. Syst. 1 (2001) 105.
[12] U.A. Paulus, A. Wokaun, G.G. Scherer, T.J. Schmidt, V. Stamenkovic, N.M. Markovic, P.N. Ross, Electrochim. Acta 47 (2002) 3787.
[13] T.J. Schmidt, H.A. Gasteiger, Rotating thin-film method for supported catalysts, in: W. Vielstich, H. Gasteiger, A. Lamm (Eds.), Handbook of Fuel Cells – Fundamentals, Technology and Applications, vol. 2, Wiley, 2003, p. 316 (Chapter 22).
[14] D. Thompsett, Pt alloys as oxygen reduction catalysts, in: W. Vielstich, H. Gasteiger, A. Lamm (Eds.), Handbook of Fuel Cells – Fundamentals, Technology and Applications, vol. 3, Wiley, Chichester, UK, 2003, p. 467 (Chapter 37).
[15] S. Mukerjee, S. Srinivasan, O_2 reduction structure-related parameters for supported catalysts, in: W. Vielstich, A. Lamm, H. Gasteiger (Eds.), Handbook of Fuel Cells – Fundamentals, Technology and Applications, vol. 2, Wiley, Chichester, UK, 2003, p. 502 (Chapter 34).
[16] T. Toda, H. Igarashi, H. Uchida, M. Watanabe, J. Electrochem. Soc. 146 (1999) 3750.
[17] G. Faubert, R. Cote, J.P. Dodelet, M. Lefevre, P. Bertrand, Electrochim. Acta 44 (1999) 2589.

[18] M. Lefevre, J.P. Dodelet, P. Bertrand, J. Phys. Chem. B 104 (2000) 11238.
[19] F. Jaouen, S. Marcotte, J.P. Dodelet, G. Lindbergh, J. Phys. Chem. B 107 (2003) 1376.
[20] M. Bron, S. Fiechter, P. Bogdanoff, H. Tributsch, Fuel Cells: Fundam. Syst. 2 (2002) 137.
[21] M. Bron, J. Radnik, M. Fieber-Erdmann, P. Bogdanoff, S. Fiechter, J. Electroanal. Chem. 535 (2002) 113.
[22] B. Sompalli, H.A. Gasteiger, M.F. Mathias, M. Scozzafava, Methods of preparing membrane electrode assemblies, US Patent 6,524,736 B1 (2003).
[23] B. Sompalli, H.A. Gasteiger, in press.
[24] T.R. Ralph, G.A. Hards, J.E. Keating, S.A. Campbell, D.P. Wilkinson, M. Davis, J. St-Pierre, M.C. Johnson, J. Electrochem. Soc. 144 (1997) 3845.
[25] U.A. Paulus, T.J. Schmidt, H.A. Gasteiger, R.J. Behm, J. Electroanal. Chem. 495 (2001) 134.
[26] D.M. Bernardi, M.W. Verbrugge, J. Electrochem. Soc. 139 (1992) 2477.
[27] T.R. Ralph, M.P. Hogarth, Plat. Met. Rev. 46 (2002) 3.
[28] T.R. Ralph, J.E. Keating, N.J. Collis, T.I. Hyde, ETSU Contract Report F/02/00038, 1997.
[29] E.A. Ticianelli, C. Derouin, S. Srinivasan, J. Electroanal. Chem. 251 (1988) 275.
[30] S. Mukerjee, S. Srinivasan, J. Electroanal. Chem. 357 (1993) 201.
[31] X. Wang, I. Hsing, P.L. Yue, J. Power Sources 96 (2001) 282.
[32] S.J. Lee, S. Mukerjee, J. McBreen, Y.W. Rho, Y.T. Kho, T.H. Lee, Electrochim. Acta 43 (1998) 3693.
[33] T. Tada, High dispersion catalysts including novel carbon supports, in: W. Vielstich, A. Lamm, H. Gasteiger (Eds.), Handbook of Fuel Cells – Fundamentals, Technology and Applications, vol. 3, Wiley, 2003, p. 481 (Chapter 38).
[34] J. Ihonen, F. Jaounen, G. Lindbergh, A. Lundblad, G. Sundholm, J. Electrochem. Soc. 149 (2002) 448.
[35] T.J. Schmidt, H.A. Gasteiger, G.D. Stab, P.M. Urban, D.M. Kolb, R.J. Behm, J. Electrochem. Soc. 146 (1999) 1296.
[36] S.L. Gojkovic, S.K. Zecevic, R.F. Savinell, J. Electrochem. Soc. 145 (1998) 3713.
[37] F. Gloaguen, P. Convert, S. Gamburzev, O.A. Velev, S. Srinivasan, Electrochim. Acta 43 (1998) 3767.
[38] J. Perez, E.R. Gonzalez, E.A. Ticianelli, Electrochim. Acta 44 (1998) 1329.
[39] W.J. Albery, M.L. Hitchman, Ring-Disc Electrodes, Clarendon Press, Oxford, 1971.
[40] V. Stamenkovic, T.J. Schmidt, P.N. Ross, N.M. Markovic, J. Phys. Chem. B 106 (2002) 11970.
[41] N.M. Markovic, H.A. Gasteiger, P.N. Ross, J. Electrochem. Soc. 144 (1997) 1591.
[42] N.M. Markovic, P.N. Ross, Surf. Sci. Rep. 45 (2002) 117.
[43] N.M. Markovic, H.A. Gasteiger, P.N. Ross, J. Phys. Chem. 100 (1996) 6715.
[44] T.D. Jarvi, T.W. Patterson, N.E. Cipollini, J.B. Hertzberg, M.L. Perry, Recoverable Performance Losses in PEMFC Spring 2003 ECS Meeting Abstracts, Abstract Number 1211, The Electrochemical Society, Paris, France, 2003.
[45] K. Kinoshita, Electrochemical Oxygen Technology, Wiley, New York, 1992.
[46] D.A. Landsman, F.J. Luczak, Catalyst studies and coating technologies, in: W. Vielstich, H. Gasteiger, A. Lamm (Eds.), Handbook of Fuel Cells, vol. 4, Wiley, 2003, p. 811 (Chapter 60).
[47] O. Antoine, Y. Bultel, R. Durand, J. Electroanal. Chem. 499 (2001) 85.
[48] V. Jalan, E.J. Taylor, J. Electrochem. Soc. 130 (1983) 2299.
[49] N.M. Markovic, H.A. Gasteiger, P.N. Ross, J. Phys. Chem. 99 (1995) 3411.
[50] M.T. Paffett, J.G. Beery, S. Gottesfeld, J. Electrochem. Soc. 135 (1988) 1431.
[51] F.J. Luczak, J. Catal. 43 (1976) 376.
[52] S. Mukerjee, S. Srinivasan, M.P. Soriaga, J. Electrochem. Soc. 142 (1995) 1409.
[53] P.N. Ross, Oxygen reduction reaction on smooth single crystal electrodes, in: W. Vielstich, H. Gasteiger, A. Lamm (Eds.), Handbook of Fuel Cells – Fundamentals, Technology and Applications, vol. 2, Wiley, 2003, p. 465 (Chapter 31).
[54] V. Jalan, D.A. Landsman, Noble metal-refractory metal alloys as catalysts and method for making, US Patent 4,186,944 (1980).
[55] D.A. Landsman, F.J. Luczak, US Patent 4,316,944 (1982).
[56] F.J. Luczak, D.A. Landsman, Ordered ternary fuel cell catalysts containing platinum and cobalt and method for making the catalysts, US Patent 4,677,092 (1987).
[57] S.S. Kocha, K. Deluca, F.J. Luczak, PtRhFe/C for PAFC, Electrochemical Society Meeting Abstracts, vol. 1, San Diego, CA, 1998, p. 34.
[58] V. Stamenkovic, T.J. Schmidt, P.N. Ross, N.M. Markovic, in press.
[59] K.A. Striebel, P.C. Andricacos, E.J. Cairns, P.N. Ross, F.R. McLarnon, J. Electrochem. Soc. 132 (1985) 2381.
[60] P.N. Ross, E.J. Cairns, K.A. Striebel, F.R. McLarnon, Electrochim. Acta 32 (1987) 335.
[61] K.-L. Hsueh, H.H. Chang, D.-T. Chin, S. Srinivasan, Electrochim. Acta 30 (1985) 1137.
[62] S. Mukerjee, S. Srinivasan, M.P. Soriaga, J. McBreen, J. Electrochem. Soc. 142 (1995) 1409.
[63] T. Okada, Effect of ionic contaminants on PEM fuel cells, in: W. Vielstich, A. Lamm, H. Gasteiger (Eds.), Handbook of Fuel Cells, Fuel Cell Technology and Applications, vol. 3, Wiley, 2003, p. 627 (Chapter 48).
[64] T. Okada, Y. Ayato, M. Yuasa, I. Sekine, J. Phys. Chem. 103 (1999) 3315.
[65] P.N. Ross, F.T. Wagner, LBL-14192: Prospects for the Development of Non-Noble Metal Catalysts for Hydrogen-Air Fuel Cells, Lawrence Berkeley Laboratory, Berkeley, CA, 1982.
[66] A.B. LaConti, M. Hamdan, R.C. McDonald, Mechanisms of membrane degradation for PEMFCs, in: W. Vielstich, H. Gasteiger, A. Lamm (Eds.), Handbook of Fuel Cells – Fundamentals, Technology and Applications, vol. 3, Wiley, Chichester, UK, 2003, p. 647 (Chapter 49).
[67] H. Jahnke, M. Schonborn, in 3 es Journees Int. d'Etude des Piles a Combustible, Bruxelles, 1969, p. 60.
[68] H. Meier, U. Tschirwitz, E. Zimmerhackl, W. Albrecht, Bundesmin. f. Verteidigung, Report FBWT 75-6, Bonn, BRD, 1975.
[69] H. Alt, H. Binder, W. Linder, G. Sandstede, J. Electroanal. Chem. 31 (1971), App 19.
[70] F.T. Wagner, H.A. Gasteiger, S.S. Kocha, T.E. Moylan, S.G. Yan, in: Proceedings of the Advanced Automotive Battery Conference, Nice, France, June 10–13, 2003.
[71] F.T. Wagner, H.A. Gasteiger, S.G. Yan, Proceedings of DOE Workshop on Non-Pt Electrocatalysts, New Orleans, LA, March 21–23, 2003. http://www.eere.energy.gov/hydrogenandfuelcells/pdfs/fred_-wagner.ppt.
[72] P.D. Beattie, V.I. Basura, S. Holdcroft, J. Electroanal. Chem. 468 (1999) 180.
[73] M. Bron, Private Communication, 2 February 2004.